FERMILAB-PUB-17/492-T
TUM-EFT 107/18

Up-, down-, strange-, charm-, and bottom-quark masses from four-flavor lattice QCD

A. Bazavov,[1] C. Bernard,[2,*] N. Brambilla,[3,4,†] N. Brown,[2] C. DeTar,[5] A.X. El-Khadra,[6,7] E. Gámiz,[8] Steven Gottlieb,[9] U.M. Heller,[10] J. Komijani,[3,4,11,‡] A.S. Kronfeld,[7,4,§] J. Laiho,[12] P.B. Mackenzie,[7] E.T. Neil,[13,14] J.N. Simone,[7] R.L. Sugar,[15] D. Toussaint,[16,¶] A. Vairo,[3,**] and R.S. Van de Water[7]

(Fermilab Lattice, MILC, and TUMQCD Collaborations)

[1]*Department of Computational Mathematics, Science and Engineering, and Department of Physics and Astronomy, Michigan State University, East Lansing, Michigan 48824, USA*

[2]*Department of Physics, Washington University, St. Louis, Missouri 63130, USA*

[3]*Physik-Department, Technische Universität München, 85748 Garching, Germany*

[4]*Institute for Advanced Study, Technische Universität München, 85748 Garching, Germany*

[5]*Department of Physics and Astronomy, University of Utah, Salt Lake City, Utah 84112, USA*

[6]*Department of Physics, University of Illinois, Urbana, Illinois 61801, USA*

[7]*Fermi National Accelerator Laboratory, Batavia, Illinois 60510, USA*

[8]*CAFPE and Departamento de Física Teórica y del Cosmos, Universidad de Granada, E-18071 Granada, Spain*

[9]*Department of Physics, Indiana University, Bloomington, Indiana 47405, USA*

[10]*American Physical Society, One Research Road, Ridge, New York 11961, USA*

[11]*School of Physics and Astronomy, University of Glasgow, Glasgow G12 8QQ, United Kingdom*

[12]*Department of Physics, Syracuse University, Syracuse, New York 13244, USA*

[13]*Department of Physics, University of Colorado, Boulder, Colorado 80309, USA*

[14]*RIKEN-BNL Research Center, Brookhaven National Laboratory, Upton, New York 11973, USA*

[15]*Department of Physics, University of California, Santa Barbara, California 93106, USA*

[16]*Physics Department, University of Arizona, Tucson, Arizona 85721, USA*

(Dated: February 13, 2018)

Abstract

We calculate the up-, down-, strange-, charm-, and bottom-quark masses using the MILC highly improved staggered-quark ensembles with four flavors of dynamical quarks. We use ensembles at six lattice spacings ranging from $a \approx 0.15$ fm to 0.03 fm and with both physical and unphysical values of the two light and the strange sea-quark masses. We use a new method based on heavy-quark effective theory (HQET) to extract quark masses from heavy-light pseudoscalar meson masses. Combining our analysis with our separate determination of ratios of light-quark masses we present masses of the up, down, strange, charm, and bottom quarks. Our results for the $\overline{\rm MS}$-renormalized masses are $m_u(2\text{ GeV}) = 2.118(38)$ MeV, $m_d(2\text{ GeV}) = 4.690(54)$ MeV, $m_s(2\text{ GeV}) = 92.52(69)$ MeV, $m_c(3\text{ GeV}) = 984.3(5.6)$ MeV, and $m_c(m_c) = 1273(10)$ MeV, with four active flavors; and $m_b(m_b) = 4197(14)$ MeV with five active flavors. We also obtain ratios of quark masses $m_c/m_s = 11.784(22)$, $m_b/m_s = 53.93(12)$, and $m_b/m_c = 4.577(8)$. The result for m_c matches the precision of the most precise calculation to date, and the other masses and all quoted ratios are the most precise to date. Moreover, these results are the first with a perturbative accuracy of α_s^4. As byproducts of our method, we obtain the matrix elements of HQET operators with dimension 4 and 5: $\overline{\Lambda}_{\rm MRS} = 552(30)$ MeV in the minimal renormalon-subtracted (MRS) scheme, $\mu_\pi^2 = 0.06(22)$ GeV^2, and $\mu_G^2(m_b) = 0.38(2)$ GeV^2. The MRS scheme [Phys. Rev. **D97**, 034503 (2018), arXiv:1712.04983 [hep-ph]] is the key new aspect of our method.

* cb@lump.wustl.edu
† nora.brambilla@ph.tum.de
‡ javad.komijani@glasgow.ac.uk
§ ask@fnal.gov
¶ doug@physics.arizona.edu
** antonio.vairo@tum.de

I. INTRODUCTION

Quark masses are fundamental parameters of QCD. They must be known accurately for precise theoretical calculations within the Standard Model, especially for testing whether quarks receive mass via Yukawa couplings to the Higgs field. Because of confinement, the quark masses can be defined only as renormalized parameters of the QCD Lagrangian. Thus, they must be determined by comparing theoretical calculations of an appropriate set of observables to experimental measurements of those observables. Lattice QCD makes it possible to calculate in a nonperturbative way simple observables, such as hadron masses. To determine the quark masses in lattice QCD, one needs to tune the bare lattice quark masses such that a suitable set of hadron masses coincide with their experimental values.

The resulting bare masses must be renormalized, preferably to a regularization independent scheme, such as the recently introduced minimal renormalon subtracted (MRS) mass [1]. One approach is to use lattice perturbation theory, but multiloop calculations are difficult so, in practice, nothing more than two-loop matching [2–4] is available in the literature. Another is to use nonperturbative renormalization to, for example, momentum-subtraction [5, 6] or finite-volume [7, 8] schemes. Finally, one can use lattice gauge theory to obtain quantities in continuum QCD and apply multiloop continuum perturbative QCD to extract the quark masses. An example of the latter is the analysis of quarkonium correlators [9]. In practice, no regularization-independent scheme is in such common use as the modified minimal subtraction ($\overline{\text{MS}}$) scheme [10] of dimensional regularization, so we shall use $\overline{\text{MS}}$ to quote results.

Our method studies how a heavy-light meson mass depends on the mass of its heavy valence (anti)quark [11–13]. Like the quarkonium correlators, our approach requires only continuum perturbation theory. On the other hand, the binding energy of a heavy-light meson is of order Λ_{QCD}, so it is necessary to use heavy quark effective theory (HQET) to separate long- and short-distance scales. In this way, we can obtain the masses of the charm and bottom quarks and, at the same time, HQET matrix elements [13]. Because this analysis uses as inputs the bare masses of the up, down, and strange quarks—tuned to reproduce the pion and kaon masses [14], it also yields the renormalized masses of these quarks.

Following Ref. [13], our analysis is based on the HQET formula for the heavy-light meson mass [15]

$$M_{H^{(*)}} = m_h + \overline{\Lambda} + \frac{\mu_\pi^2}{2m_h} - d_{H^{(*)}} \frac{\mu_G^2(m_h)}{2m_h} + \text{O}\left(m_h^{-2}\right), \tag{1.1}$$

where $M_{H^{(*)}}$ is the pseudoscalar (vector) meson mass; m_h is the heavy-quark mass; and $\overline{\Lambda}$, μ_π^2, and $\mu_G^2(m_h)$ are matrix elements of HQET operators with dimension 4 and 5. The last three correspond to the energy of the light quarks and gluons, the heavy quark's kinetic energy, and the spin-dependent chromomagnetic energy, with coefficient $d_H = 1$ for pseudoscalar mesons and $d_{H^*} = -\frac{1}{3}$ for vector mesons. The chromomagnetic operator has an anomalous dimension, known to three loops [16], so $\mu_G^2(m_h)$ depends logarithmically on the mass m_h. The strategy is to use lattice QCD to compute $M_H^{(*)}$ as a function of m_h and fit Eq. (1.1) to distinguish the terms on the right-hand side including, in principle, higher orders in $1/m_h$ [13].

The utility of Eq. (1.1) rests on the definition of the quark mass m_h. In HQET, the natural definition is the pole mass (also known as the on-shell mass). Although the pole mass is infrared finite [17] and gauge independent [17, 18] at every order in perturbation theory, its value is ambiguous when all orders are considered [19, 20]. At large orders,

the coefficients of the self energy grow factorially, and a possible interpretation via Borel summation is obstructed by a series of renormalon singularities [19, 20]. This behavior is a manifestation of the strongly-coupled long-range gluon field that, remarkably, appears in perturbation theory. Note that because M_H is unambiguous, the ambiguity in m_h must be cancelled by those in $\overline{\Lambda}$, μ_π^2, and higher-dimension terms.[1]

To address this problem, some of us introduced the minimal renormalon-subtracted (MRS) mass in a companion paper [1]. It is defined by Eqs. (2.24) of Ref. [1],

$$m_{\rm MRS} = \overline{m}\left(1 + \sum_{n=0}^{\infty} [r_n - R_n]\,\alpha_s^{n+1}(\overline{m}) + J_{\rm MRS}(\overline{m})\right), \tag{1.2}$$

where $\overline{m} = m_{\overline{\rm MS}}(m_{\overline{\rm MS}})$, the r_n are the coefficients relating the $\overline{\rm MS}$ mass to the pole mass, R_n denote their asymptotic behavior, and $J_{\rm MRS}(\overline{m})$, which is defined in Eqs. (2.25) and (2.26) of Ref. [1], is the unambiguous part of the Borel sum of $\sum R_n \alpha_s^{n+1}$. To compute $m_{\rm MRS}$ one uses the known behavior of the R_n [21–23], including their overall normalization [23]. In deriving Eq. (1.2), Ref. [1] puts the leading renormalon ambiguity into a specific quantity of order $\Lambda_{\overline{\rm MS}}$, denoted δm, and transfers it from m_h to $\overline{\Lambda}$. Below we write $m_{h,\rm MRS}$ and $\overline{\Lambda}_{\rm MRS}$ to denote the unambiguous definitions of m_h and $\overline{\Lambda}$ in the MRS scheme.

A second feature of our technique may seem almost trivial. In Eq. (4.7), Ref. [1] rewrites $m_{h,\rm MRS}$ as

$$m_{h,\rm MRS} = \frac{m_{r,\overline{\rm MS}}(\mu)\,am_h}{m_{h,\overline{\rm MS}}(\mu)\,am_r} m_{h,\rm MRS} \tag{1.3a}$$

$$= m_{r,\overline{\rm MS}}(\mu)\frac{\overline{m}_h}{m_{h,\overline{\rm MS}}(\mu)}\frac{m_{h,\rm MRS}}{\overline{m}_h}\frac{am_h}{am_r}, \tag{1.3b}$$

where am_r is the bare mass (in lattice units) of staggered fermions, and the subscript r labels a reference mass; see Sec. III. Owing to the remnant chiral symmetry of staggered fermions, the first factor in Eq. (1.3a) is $1+{\rm O}(a^2)$. In Eq. (1.3b), the factors are, respectively, a convenient fit parameter, the factor to run from scale μ to $\overline{m}_h$, the quantity in the big parentheses in Eq. (1.2), and the ratio of the freely chosen heavy-quark lattice mass to the reference mass. Equation (1.3) plays a key role: with r_n for $\overline{\rm MS}$ in Eq. (1.2), the first factor in Eq. (1.3b) is in the $\overline{\rm MS}$ scheme; with $J_{\rm MRS}$ removing the leading renormalon ambiguity, the product on the right-hand side of Eq. (1.3b) is indeed the MRS mass. By taking $m_r = 0.4m_s$ (the so-called $p4s$ approach), the analysis yields m_s as well as the heavy-quark masses m_c and m_b.

The third important feature of our work is a data set with a wide range of lattice spacing, heavy-quark mass, and light valence and sea masses. These data, which were generated in a companion project to compute the B- and D-meson decay constants [14], are very precise, with statistical errors of 0.005–0.12%. It is very challenging to take advantage of the statistical power and parameter range of the data set. In this paper, we use heavy-meson rooted all-staggered chiral perturbation theory [24] (HMrASχPT) to describe the dependence of the heavy-light pseudoscalar meson masses on the light mesons. To make possible a fit to lattice data, Ref. [1] combined the next-to-leading-order HMrASχPT with the MRS mass to write heavy-light meson masses as a function of lattice spacing and heavy-

[1] By forming the spin average, $\frac{1}{4}(M_H + 3M_{H^*})$, and spin difference, $M_{H^*} - M_H$, it is easy to see that spin-independent and spin-dependent ambiguities are distinct.

and light-quark masses. The fit function, by construction, has the correct nonanalytic form in the chiral and HQET limits. Here, it is extended with enough analytic terms to mimic higher-order corrections and obtain a good fit.

We use twenty ensembles generated by the MILC Collaboration [25–27] with four flavors of sea quarks using the highly-improved staggered quark (HISQ) action [28] and a one-loop [29] tadpole-improved [30] Symanzik-improved gauge action [31–35]. The algorithm for the quark determinant uses the fourth-root procedure to remove the unwanted taste degrees of freedom [36–49]. A thorough description of the simulation program can be found in Ref. [26]. Since then, the simulations have been extended to smaller lattice spacings; up-to-date details are in Ref. [14]. Our procedures for calculating pseudoscalar meson correlators and for finding masses and amplitudes from these correlators are described in Refs. [14, 50]. The amplitudes are used in Ref. [14] to calculate the decay constants of B and D mesons, and the corresponding meson masses are used here.

A preliminary report of this analysis can be found in Ref. [51]. Instead of the MRS mass, at that time we used the renormalon-subtracted (RS) mass [22], which also subtracts the leading renormalon ambiguity but at the same time introduces a factorization scale ν_f. In principle, the $\overline{\rm MS}$ masses emerging from Eqs. (1.3) and (1.1) should not depend on ν_f, but we found more dependence than one would like. Moreover, it turns out to be necessary to introduce three scales in all, $\nu_f < \mu < m_h$, with μ being used for α_s [51]. For that reason, we prefer the MRS over the RS mass.

This paper is organized as follows. Section II contains a description of the lattice-QCD simulations, focusing on the way we eliminate the lattice scale in favor of physical units. In Sec. III, we present our function of quark masses and lattice spacing that describes masses of heavy-light pseudoscalar mesons. In Sec. IV, we perform a combined-correlated fit to the meson masses; the fit is then extrapolated to the continuum and interpolated to physical values of the light quark masses. In Sec. V, we present our final results for the masses of the strange, charm and bottom quarks as well as quark mass ratios m_c/m_s, m_b/m_s, and m_b/m_c. Combining our results with our separate determination of the quark-mass ratios m_u/m_d and m_s/m_l, where $m_l \equiv \frac{1}{2}(m_u+m_d)$, we also report the up- and down-quark masses. In addition, we present our lattice-QCD determinations of $\overline{\Lambda}_{\rm MRS}$, μ_π^2, and $\mu_G^2(m_b)$ as well as flavor splittings and low-energy constants of heavy-meson chiral perturbation theory. Section VI compares our main results with work in the literature and offers some remarks on further work. An appendix gives the correlation matrices of the MRS masses of the charm and bottom quarks with HQET matrix elements, and of the charm-quark mass and quark-mass ratios.

II. SIMULATIONS SUMMARIZED

The lattice data used in this work come from the same correlation functions used to determine leptonic decay constants of charmed and b-flavored mesons in a companion paper [14]. For a full description of the simulation, the reader should consult Ref. [14]. Here we provide a brief summary.

We employ a data set that includes ensembles with five values of lattice spacings ranging from approximately 0.12 fm to 0.03 fm, enabling good control over the continuum extrapolation. Ensembles at a sixth lattice spacing, approximately 0.15 fm, are used only to estimate the continuum extrapolation error. The data set includes ensembles with the light (up-down), strange, and charm sea-masses close to their physical values ("physical-mass

ensembles") at all but the smallest lattice spacing, 0.03 fm. The data set also includes ensembles where either the mass of light sea quarks is heavier than in nature, or the mass of the strange sea quark is lighter than in nature, or both. As in Ref. [14], we set the scale of the lattice spacing a with a two-step procedure that uses the value of f_π from the Particle Data Group (PDG), $f_{\pi,\mathrm{PDG}} = 130.50(13)$ MeV [52], combined with the so-called $p4s$ method.

The first step in the scale-setting procedure takes $f_{\pi,\mathrm{PDG}}$ to set the overall scale on each *physical-mass* ensemble. On these ensembles, we tune the valence light, strange, and charmed quark masses to reproduce the pion, kaon, and D_s-meson masses. Then we calculate M_{p4s} and f_{p4s}, which are the mass and decay constant of a pseudoscalar meson with both valence-quark masses set equal to $m_{p4s} \equiv 0.4m_s$. We then form the ratio $R_{p4s} \equiv f_{p4s}/M_{p4s}$ and take the continuum limit of f_{p4s} and R_{p4s}. These values and those of the quark mass ratios are then used as inputs to the second step of the procedure, which we call the $p4s$ method. In the $p4s$ method, the values of am_{p4s} and af_{p4s} are calculated on a given physical-mass ensemble, with $a \neq 0$, by adjusting the valence-quark mass until af_{p4s}/aM_{p4s} equals the physical-mass continuum limit of R_{p4s}:

$$R_{p4s}(m_{p4s}; \{\tfrac{1}{2}(m_u + m_d), m_s, m_c\}; a) = R_{p4s}(0.4m_s; \{\tfrac{1}{2}(m_u + m_d), m_s, m_c\}; 0). \tag{2.1}$$

In the $p4s$ method, all ensembles at the same bare gauge coupling, $\beta = 10/g_0^2$, as a given physical-mass ensemble are chosen to have the same lattice spacing a and the same am_{p4s}. This choice is known as a *mass-independent scale-setting scheme*.

At $a \approx 0.03$ fm, we have only a $0.2m_s$ ensemble, so this procedure cannot be carried out. In this case, we rely on the derivatives with respect to a, which are given in Ref. [50].

III. CONSTRUCTION OF THE FIT FUNCTION

In this section, we discuss in detail how to construct a function of quark masses and lattice spacing that describes masses of heavy-light pseudoscalar mesons. To this end, we use three effective field theories (EFTs), HQET, and HMrASχPT, as mentioned already, and the Symanzik effective theory of cutoff effects [34, 53, 54]. We start with the merger of HQET and HMrASχPT [1] and incorporate generic lattice-spacing dependence, as well as higher-order terms in HQET and HMrASχPT. Putting everything together, we obtain an EFT fit function for masses of heavy-light pseudoscalar mesons.

A. Leading-order χPT

Let us start with fixing our notation for quark masses associated with lattice ensembles with 2+1+1 flavors of quarks. We use m_l', m_s', and m_c' to denote the simulation masses of the light (up-down), strange, and charm quarks, respectively; without the primes, we use $m_l = \frac{1}{2}(m_u + m_d)$, m_s, and m_c to denote the correctly tuned masses of the corresponding quarks; last, we use m_q to denote a generic light quark mass. Further, we use $H_x^{(*)}$ to denote a generic heavy-light pseudoscalar (vector) meson composed of a light valence quark x and a heavy valence antiquark $\bar{h}$. We also use $m_{h,\mathrm{MRS}}$, $m_{h,\overline{\mathrm{MS}}}$, and am_h to denote the MRS, $\overline{\mathrm{MS}}$, and bare masses of antiquark $\bar{h}$, respectively. The relations between $m_{h,\mathrm{MRS}}$, $m_{h,\overline{\mathrm{MS}}}$, and am_h are discussed in Sec. III C.

In HMrASχPT, the mass of $H_x^{(*)}$ meson is described by Eq. (4.2) of Ref. [1]

$$M_{H_x^{(*)}}(m_x;\{m_l',m_l',m_s'\};a) = m_{h,\mathrm{MRS}} + \overline{\Lambda}_{\mathrm{MRS}} + \frac{\mu_\pi^2 - d_{H^{(*)}}\mu_G^2(m_h)}{2m_{h,\mathrm{MRS}}} + 2\lambda_1 B_0 m_x \\ + 2\lambda_1' B_0(2m_l' + m_s') + \delta M_{H_x^{(*)}}(m_x;\{m_l',m_l',m_s'\};a) - \mathcal{C}^{(*)}, \tag{3.1}$$

where B_0 is the low energy constant (LEC) in the relation $m_\pi^2 = B_0(m_u + m_d)$ between the pion mass and the quark mass; $d_{H^{(*)}} = 1$ $(-\frac{1}{3})$ for pseudoscalar (vector) mesons; λ_1 and λ_1' are LECs that appear in (continuum) heavy-meson chiral perturbation theory (HMχPT) [55]; and $\delta M_{H_x^{(*)}}$ is the one-loop corrections to the mass of the $H_x^{(*)}$ meson in HMrASχPT [1]. The arguments of $M_{H_x^{(*)}}$ and $\delta M_{H_x^{(*)}}$ in Eq. (3.1) correspond to the light valence-quark mass; the set of three light sea-quark masses, which are not necessarily tuned to their physical values; and the lattice spacing a. As usual for a one-loop χPT result, δM_{H_x} contains a term nonanalytic as $m_\pi^2 \to 0$ (a "chiral log"). For the pseudoscalar mesons with $(2+1)$ light flavors in the sea, we have.

$$\begin{aligned}\delta M_{H_x} = -\frac{3g_\pi^2}{16\pi^2 f^2}\Bigg\{ & \frac{1}{16}\sum_{\mathcal{S},\Xi'} K_1(m_{\mathcal{S}x_{\Xi'}}, \Delta^* + \delta_{\mathcal{S}x}) \\ & + \frac{1}{3}\sum_{j\in\mathcal{M}_I^{(2,x)}} \frac{\partial}{\partial m_{X_I}^2}\left[R_j^{[2,2]}(\mathcal{M}_I^{(2,x)};\mu_I^{(2)})K_1(m_j,\Delta^*)\right] \\ & + \left(a^2\delta_V' \sum_{j\in\hat{\mathcal{M}}_V^{(3,x)}} \frac{\partial}{\partial m_{X_V}^2}\left[R_j^{[3,2]}(\hat{\mathcal{M}}_V^{(3,x)};\mu_V^{(2)})K_1(m_j,\Delta^*)\right] + [V\to A]\right)\Bigg\} \\ & + a^2\frac{3g_\pi^2}{16\pi^2 f^2}\left[\lambda'_{a^2}\bar{\Delta}\sum_{\mathcal{S}}\delta_{\mathcal{S}x} + \lambda_{a^2}\Delta^*\left(3\bar{\Delta} - \tfrac{1}{3}\Delta_I + \delta_V' + \delta_A'\right)\right].\end{aligned} \tag{3.2}$$

where the indices $\mathcal{S}$ and Ξ run over light sea-quark flavors and meson tastes, respectively; $M_{\mathcal{S}x,\Xi}$ is the mass of the pseudoscalar meson with taste Ξ and flavors $\mathcal{S}$ and x; Δ^* is the lowest-order hyperfine splitting; $\delta_{\mathcal{S}x}$ is the flavor splitting between a heavy-light meson with light quark of flavor $\mathcal{S}$ and one of flavor x; g_π is the H-H^*-π coupling; δ_A' and δ_V' are the taste-breaking hairpin parameters; $a^2\bar{\Delta}$ is the mean-squared pion taste splitting; and λ_{a^2} and λ'_{a^2} are parameters in SχPT related to taste breaking in meson masses. Definitions of the residue functions $R_j^{[n,k]}$, the sets of masses in the residues, and the chiral-log function K_1 at infinite and finite volumes are given in Ref. [1] and references therein. The expression for $\delta M_{H_x^*}$ is also given in Ref. [1], but because we have lattice data only for pseudoscalar mesons, it is not needed here.

In Eq. (3.1), we set

$$\mathcal{C}^{(*)} = 2\lambda_1 B_0 m_q + 2\lambda_1' B_0(2m_l + m_s) + \delta M_{H_q^{(*)}}(m_q;\{m_l,m_l,m_s\};0) \tag{3.3}$$

so that in the continuum limit the usual expression

$$M_{H_q^{(*)}}(m_q;\{m_l,m_l,m_s\};0) = m_{h,\mathrm{MRS}} + \overline{\Lambda}_{\mathrm{MRS}} + \frac{\mu_\pi^2 - d_{H^{(*)}}\mu_G^2(m_h)}{2m_{h,\mathrm{MRS}}} \tag{3.4}$$

is recovered for physical values of sea-quark masses and $m_x = m_q$. With this choice for $\mathcal{C}$, the values that we obtain for $\overline{\Lambda}_{\rm MRS}$, μ_π^2 and $\mu_G^2(m_h)$ are readily applicable for calculations in HQET.[2] In this work, we set $m_q = \frac{1}{2}(m_u + m_d)$, and we report $\overline{\Lambda}_{\rm MRS}$, μ_π^2 and $\mu_G^2(m_h)$ for this choice.

At this stage, the fit parameters are $m_{r,\overline{\rm MS}}(\mu = 2\ {\rm GeV})$ via Eq. (1.3), $\overline{\Lambda}_{\rm MRS}$, the kinetic energy μ_π^2, the chromomagnetic energy $\mu_G^2(m_b)$ from which we obtain $\mu_G^2(m_h)$ as in Eq. (3.6) below, and the LECs λ_1, λ_1', λ_{a^2}, and λ_{a^2}'. Ideally, one would have data for both pseudoscalar- and vector-meson masses, and then one could set up separate fits for spin-independent and spin-dependent terms. In this work, however, only the pseudoscalar masses are available. The experimental masses of the B^* and B meson can be used to estimate

$$\mu_G^2(m_b) \approx \frac{3}{4}(M_{B^*}^2 - M_B^2) = 0.36\ {\rm GeV}^2, \tag{3.5}$$

which neglects contributions to the hyperfine splitting suppressed by a power of $1/m_b$. The chromomagnetic operator has an anomalous dimension, however, so we obtain $\mu_G^2(m_h)$ in Eq. (3.1) with

$$\mu_G^2(m_h) = \frac{C_{\rm cm}(m_h)}{C_{\rm cm}(m_b)}\mu_G^2(m_b), \tag{3.6}$$

using the three-loop relation [16] for the Wilson coefficient $C_{\rm cm}(m_h)$. For four active flavors,

$$C_{\rm cm}(m_h) = \alpha_s^{9/25}\left(1 + 0.672355\alpha_s + 1.284\alpha_s^2\right), \tag{3.7}$$

where $\alpha_s = \alpha_{\overline{\rm MS}}(\overline{m}_h)$.

As discussed in Sec. I and Ref. [1], the matrix elements of HQET suffer in general from ambiguities related to renormalon singularities, although the ambiguities cancel in observables such as the meson mass. For instance, the ambiguity in $\overline{\Lambda}$ cancels the leading-renormalon ambiguity in the pole mass. By construction, only the leading renormalon is removed to define the MRS mass. In principle, renormalon ambiguities in μ_π^2 and $\mu_G^2(m_h)$ remain. In practice, numerical investigation indicates that the subleading infrared renormalon of the pole mass is small [1], which implies that the corresponding renormalon ambiguity in μ_π^2 is not large. Moreover, the leading spin-dependent renormalon in μ_G^2 is suppressed by a further power of $1/m_h$.

B. Higher-order terms in χPT

Because we have very precise data with statistical errors of 0.005–0.12%, we can anticipate that NLO χPT is not enough to describe fully the quark-mass dependence, especially for data with m_x near m_s. We therefore extend the function given in Eq. (3.1) by adding higher-order analytic corrections in powers of light quark masses and in inverse powers of the heavy quark mass. For the expansion in inverse powers of the heavy-quark mass, we introduce the dimensionless variable

$$w_h = \frac{\Lambda_{\rm HQET}}{m_{h,\rm MRS}}, \tag{3.8}$$

[2] Note that in the context of Eq. (3.4), the matrix elements $\overline{\Lambda}_{\rm MRS}$, μ_π^2 and $\mu_G^2(m_h)$ depend on the light-quark masses.

with $\Lambda_{\rm HQET} = 600$ MeV. Then the natural size of coefficients of the $1/m_h$ corrections is of order 1. For expansion in light quark masses, following Refs. [14, 50], we define dimensionless quark masses, which are natural expansion parameters in χPT:

$$x_q \equiv \frac{B_0}{4\pi^2 f_\pi^2} m_q, \tag{3.9}$$

where q can be either the valence or sea light quarks. For simplicity, we drop the primes on the simulation x_qs. The quark masses in the formula for δM_{H_x} can also be expressed in terms of $\{x_x, x_l, x_s\}$.

We include all mass-dependent analytic terms at order x_q^2 by adding

$$f_\pi \left[q_1 x_x^2 + q_2 x_x (2x_l + x_s) + q_3 (2x_l + x_s)^2 + q_4 (2x_l^2 + x_s^2) \right] \tag{3.10}$$

to the expression for M_{H_x} in Eq. (3.1). With f_π to set the overall scale of these higher-order terms, the coefficients q_i become of order 1 or less. We also include all mass-dependent analytic terms at order x_q^3, namely

$$x_x^3,\ x_x^2(2x_l{+}x_s),\ x_x(2x_l{+}x_s)^2,\ x_x(2x_l^2{+}x_s^2),\ (2x_l{+}x_s)^3,\ (2x_l{+}x_s)(2x_l^2{+}x_s^2),\ 2x_l^3{+}x_s^3. \tag{3.11}$$

In practice, one can expect the terms without x_x to be less important, but we keep all of them for consistent power counting.

To improve the expansion in inverse powers of the heavy quark, we add

$$\Lambda_{\rm HQET} \left(\rho_1 w_h^2 + \rho_2 w_h^3 + \rho_3 w_h^4 \right) \tag{3.12}$$

with three fit parameters ρ_i to the right-hand side of Eq. (3.1). We also add w_h and w_h^2 corrections to the LECs λ_1, λ_1' and g_π; and w_h corrections to the fit parameters q_i in Eq. (3.10).

The heavy quark mass also affects the hyperfine splitting Δ^* and the flavor splitting δ_{sx} in Eq. (3.2). Although we could express these quantities in terms of $\mu_G^2(m_h)$ and λ_1, we exploit the experimental values for the hyperfine splittings and flavor splittings in the D and B systems to calculate Δ^* and δ_{sx} for different quark masses. See our companion paper on decay constants [14] for details.

We now discuss the effects of mistuning in the sea charm-quark mass m_c'. The effects can be divided into two parts: the effects on the pole mass (and, hence, the MRS mass) and the effects on the effective theory after the charm quark is integrated out. The former effects are taken into account in calculating the MRS mass from the $\overline{\rm MS}$ mass; cf. Eq. (3.24). We treat the latter effects as in Ref. [14]. We use $\Lambda_{\rm QCD}^{(3)}(m_c')$ to denote the effective value of $\Lambda_{\rm QCD}$ when the charm quark with mass m_c' is integrated out. At leading order in weak-coupling perturbation theory, one obtains [56, Eq. (1.114)]

$$\frac{\Lambda_{\rm QCD}^{(3)}(m_c')}{\Lambda_{\rm QCD}^{(3)}(m_c)} = \left(\frac{m_c'}{m_c} \right)^{2/27}, \tag{3.13}$$

where m_c is the correctly tuned value of charm-quark mass. Assuming $m_c' \approx m_c$, we take the effects of the mistuned mass m_c' into account by multiplying $\overline{\Lambda}_{\rm MRS}$ with

$$\left(\frac{m_c'}{m_c} \right)^{2/27} \left(1 + \frac{2k_1'}{27} \frac{m_c' - m_c}{m_c'} \right), \tag{3.14}$$

where the extra fit parameter k_1' describes higher-order corrections to Eq. (3.13).

We must also include generic lattice artifacts in our analysis. Taste-breaking discretization errors from staggered fermions are already included in Eq. (3.2). In addition to these effects, various discretization errors, from gluons for example, must be taken into account. We include the leading lattice artifacts for $\overline{\Lambda}_{\rm MRS}$ by replacing.

$$\overline{\Lambda}_{\rm MRS} \to \overline{\Lambda}_{\rm MRS}\left[1 + \bar{c}_1\alpha_s(a\Lambda)^2 + \bar{c}_2(a\Lambda)^4\right], \tag{3.15}$$

where Λ is the scale of generic discretization effects, set to 600 MeV in this analysis. The factor of α_s in the second-order term arises because the HISQ action is tree-level improved to order a^2. Note that $\overline{\Lambda}_{\rm MRS}$ is not affected by heavy-quark discretization errors. As discussed in the Appendices of Ref. [14], at leading order (LO) in HQET, heavy-quark discretization errors only affect the normalization of the heavy-quark state. Thus, $\overline{\Lambda}_{\rm MRS}$ and also λ_1, λ_1' and g_π at leading order in $1/m_h$ are free of heavy-quark discretization errors. For λ_1 we replace

$$\lambda_1 \to \lambda_1\left[1 + c_1\alpha_s(a\Lambda)^2 + c_2(a\Lambda)^4 + c_3 w_h\alpha_s(am_h)^2\right], \tag{3.16}$$

where the c_3 term is added to incorporate effects of heavy-quark discretization errors. We incorporate similar corrections for λ_1' and g_π. Finally, we add $\alpha_s(a\Lambda)^2$ and $\alpha_s(am_h)^2$ corrections to μ_π^2 and $\mu_G^2(m_b)$; and $\alpha_s(a\Lambda)^2$ corrections to the parameters q_i in Eq. (3.10).

C. Heavy-quark mass

Although the MRS mass is the key to our interpretation of the HQET mass formula, as indicated in Eq. (1.3) we arrange the fit to yield the $\overline{\rm MS}$ mass. For $am \ll 1$, the relation between the $\overline{\rm MS}$ and bare masses is

$$m_{\overline{\rm MS}}(\mu) = \frac{am}{a}\left\{1 + \alpha_s\left[-(2/\pi)\log(a\mu) + k_0 + k_1(am)^2 + \cdots\right] + {\rm O}(\alpha_s^2)\right\}, \tag{3.17}$$

where a in the denominator is set from the scale setting quantity (here f_{p4s}, as described in Sec. II). With staggered fermions, there is no additive mass renormalization, and to eliminate tree-level discretization errors from Eq. (3.17), we take the mass am to be the tree-level pole mass.[3] Taking the ratio between two masses[4]

$$\frac{m_{h,\overline{\rm MS}}(\mu)}{m_{r,\overline{\rm MS}}(\mu)} = \frac{am_h}{am_r}\left(1 + \alpha_{\overline{\rm MS}}(\mu)\left\{k_1\left[(am_h)^2 - (am_r)^2\right] + \cdots\right\} + \cdots\right), \tag{3.18}$$

where the dots stand for higher-order terms in a^2 and α_s. In fact, each higher order in α_s is also multiplied by a quantity of order a^2, as stated in the Introduction. In this analysis, we set the reference-quark mass m_r to $m_{p4s} \equiv 0.4m_s$ and the scale of the $\overline{\rm MS}$ scheme to $\mu = 2$ GeV. Thus, $m_{p4s,\overline{\rm MS}}(2\ {\rm GeV})$ is a free parameter left to be determined in the fit to lattice data; cf. Eq. (1.3b).

To incorporate further heavy-quark discretization effects into Eq. (3.18), we multiply the right-hand side of Eq. (1.3b) by

$$\left[1 + \alpha_{\overline{\rm MS}}(2\ {\rm GeV})\sum_{n=1}^{4} k_n x_h^n\right], \tag{3.19}$$

[3] The exact relation between m_0 and m can be found in Appendix A of Ref. [14].

[4] For Wilson fermions with order-a improvement, the following arguments hold for the mass defined through the axial Ward identity, apart from details about the lattice artifacts.

where the dimensionless coefficients k_n are free fit parameters, and

$$x_h = (2am_h/\pi)^2 - (2am_{p4s}/\pi)^2 \approx (2am_h/\pi)^2 \,. \tag{3.20}$$

We multiply am_h by a factor of $2/\pi$ so that the parameters k_n become of order 1, based on the radius of convergence of various tree-level formulas for the HISQ action; see Appendix A of Ref. [14]. Because $(am_{p4s}/am_c)^2 \approx 0.001$, the effects of a nonzero value of am_{p4s} are negligible compared with the heavy-quark discretization effects. To incorporate generic lattice-spacing dependence into our analysis, we additionally multiply the right-hand side of Eq. (1.3b)

$$\left[1 + \tilde{c}_1\alpha_s(a\Lambda)^2 + \tilde{c}_2(a\Lambda)^4 + \tilde{c}_3(a\Lambda)^6\right] . \tag{3.21}$$

To complete our approach to introducing $m_{p4s,\overline{\rm MS}}(2\text{ GeV})$ via $m_{h,\rm MRS}$, we must describe the calculation of the second and third factors in Eq. (1.3b). The second factor simply uses the anomalous dimension to run from $\mu = 2$ GeV to the self-consistent scale $\overline{m}_h \equiv m_{h,\overline{\rm MS}}(\overline{m}_h)$

$$\frac{\overline{m}_h}{m_{h,\overline{\rm MS}}(\mu)} = \frac{C\left(\alpha_{\overline{\rm MS}}(\overline{m}_h)\right)}{C\left(\alpha_{\overline{\rm MS}}(\mu)\right)}, \tag{3.22}$$

where with four active flavors [57]

$$C(\pi u) = u^{12/25}\left[1 + 1.01413u + 1.38921u^2 + 1.09054u^3 + 5.8304u^4 + \mathrm{O}(u^5)\right] . \tag{3.23}$$

The coefficient of u^4 is obtained from the five-loop results for the quark-mass anomalous dimension [57] and beta function [58]. Finally, the third factor in Eq. (1.3b) is simply the relation derived in Ref. [1], which at the four-loop level reads

$$\frac{m_{h,\rm MRS}}{\overline{m}_h} = 1 + \sum_{n=0}^{3}\left[r_n - R_n\right]\alpha_s^{n+1}(\overline{m}_h) + J_{\rm MRS}(\overline{m}_h) + \frac{\Delta m_{(c)}}{\overline{m}_h} + \mathrm{O}(\alpha_s^5), \tag{3.24}$$

where the r_n are known through order α_s^4 [59, 60]; the R_n depend only on the coefficients of the beta function [21, 23] up to an overall normalization, which is given in Ref. [23]; the function $\overline{m}J_{\rm MRS}(\overline{m}) = \mathcal{J}_{\rm MRS}(\overline{m})$ appears in the definition of the MRS mass [1]; and $\Delta m_{(c)}$ contains the contribution from the charm sea quark. Because the nonzero mass of the charmed sea quark cuts off the infrared region that is the origin of factorial growth in the r_n [61], we subtract the renormalon with three massless active quarks and lump the charmed loops' contributions into $\Delta m_{(c)}$ [62].

The detailed formulas for $\mathcal{J}_{\rm MRS}(\overline{m})$ and $\Delta m_{(c)}$ can be found in Ref. [1]. The crucial aspects of Eq. (3.24) for the fits of the next section is that the renormalon-subtracted perturbative coefficients are small: $r_n - R_n = (0.1106, 0.0340, 0.0966, 0.0162)$ for $n = (0, 1, 2, 3)$ and three active flavors. The Borel resummed renormalon is computed from a function with a convergent expansion in $1/\alpha_s$. (In fact, our implementation of one of the factors in $\mathcal{J}_{\rm MRS}$ uses the convergent expansion until it saturates to numerical precision.)

D. Summary formulas

In summary, we fit our data for $aM(m_h, m_x; \{m'_l, m'_l, m'_s\}; a)$ to

$$\left.\frac{aM}{af_{p4s}}\right|_{\rm data} f_{p4s} = \mathcal{F}, \tag{3.25}$$

where $\mathcal{F}$ is the fit function and f_{p4s} is in the continuum limit. From the preceding subsections [with free fit parameters in blue (arXiv)]:

$$\begin{aligned}\mathcal{F} = \breve{m}_{h,\mathrm{MRS}} &+ \breve{\overline{\Lambda}}_{\mathrm{MRS}} + \frac{\breve{\mu}_\pi^2}{2m_{h,\mathrm{MRS}}} - \frac{\breve{\mu}_G^2(m_b)}{2m_{h,\mathrm{MRS}}}\frac{C_{\mathrm{cm}}(m_h)}{C_{\mathrm{cm}}(m_b)} \\ &+ 2\breve{\lambda}_1 B_0(m_x - m_l) + 2\breve{\lambda}_1' B_0(2m_l' + m_s' - 2m_l - m_s) \\ &+ \delta M_{H_x}(m_x; \{m_l', m_l', m_s'\}; a) - \delta M_{H_l}(m_l; \{m_l, m_l, m_s\}; 0) \\ &+ \Lambda_{\mathrm{HQET}}\left[\rho_1 w_h^2 + \rho_2 w_h^3 + \rho_3 w_h^4\right] \\ &+ f_\pi\left[\sum_{i=1}^{4} q_i\left(1 + q_i' w_h + \tilde{q}_i \alpha_s y^2\right) x_i^2 + \sum_{j=5}^{11} q_j x_j^3\right],\end{aligned} \tag{3.26}$$

where $y = (a\Lambda)^2$ and $w_h = \Lambda_{\mathrm{HQET}}/m_{h,\mathrm{MRS}}$. The HMrAS$\chi$PT self energy δM_{H_x} depends on f, λ_{a^2}, λ_{a^2}', $\breve{g}_\pi$, δ_V', and δ_A', as well as Δ^* and taste-independent δ_{Sx}. The breved quantities are

$$\breve{\overline{\Lambda}}_{\mathrm{MRS}} = \overline{\Lambda}_{\mathrm{MRS}}\left(1 + \bar{c}_1\alpha_s y + \bar{c}_2 y^2\right)\left(\frac{m_c'}{m_c}\right)^{2/27}\left(1 + k_1'\frac{\delta m_c'}{m_c}\right), \tag{3.27a}$$

$$\breve{\lambda}_1 = \lambda_1\left(1 + c_1\alpha_s y + c_2 y^2 + c_3\bar{w}_h\alpha_s y + c_4\bar{w}_h + c_5\bar{w}_h^2 + c_6\bar{w}_h^3\right), \tag{3.27b}$$

$$\breve{\lambda}_1' = \lambda_1'\left(1 + c_1'\alpha_s y + c_2' y^2 + c_3'\bar{w}_h\alpha_s y + c_4'\bar{w}_h + c_5'\bar{w}_h^2 + c_6'\bar{w}_h^3\right), \tag{3.27c}$$

$$\breve{g}_\pi = g_\pi\left(1 + g_1\alpha_s y + g_2 y^2 + g_3\bar{w}_h\alpha_s y + g_4\bar{w}_h + g_5\bar{w}_h^2 + g_5\bar{w}_h^3\right), \tag{3.27d}$$

$$\breve{\mu}_\pi^2 = \mu_\pi^2\left(1 + p_\pi\alpha_s y + r_\pi\alpha_s x_h^2\right), \tag{3.27e}$$

$$\breve{\mu}_G^2(m_b) = \mu_G^2(m_b)\left(1 + p_G\alpha_s y + r_G\alpha_s x_h^2\right), \tag{3.27f}$$

where $\bar{w}_h = w_h - \Lambda_{\mathrm{HQET}}/m_{c,\mathrm{MRS}}$; further

$$\begin{aligned}\breve{m}_{h,\mathrm{MRS}} = m_{p4s,\overline{\mathrm{MS}}}(2\ \mathrm{GeV})&\left[\frac{C(\alpha_{\overline{\mathrm{MS}}}(\overline{m}_h))}{C(\alpha_{\overline{\mathrm{MS}}}(2\ \mathrm{GeV}))}\right]_{\text{Eq. (3.23)}}\left[\frac{m_{h,\mathrm{MRS}}}{\overline{m}_h}\right]_{\text{Ref. [1]}}\left[\frac{am_{0h}}{am_{0,p4s}}\right]_{\mathrm{sim}}\times \\ &\left(1 + \alpha_{\overline{\mathrm{MS}}}(2\ \mathrm{GeV})\sum_{n=1}^{4} k_n x_h^n\right)\times\left(1 + \tilde{c}_1\alpha_s y + \tilde{c}_2 y^2 + \tilde{c}_3 y^3\right).\end{aligned} \tag{3.28}$$

Thus, there are 61 free parameters, 4 parameters [f, g_π, $\mu_G^2(m_b)$, and, in $m_{h,\mathrm{MRS}}/\overline{m}_h$, R_0] with external priors, and 2 hairpin parameters (δ_V' and δ_A') from light-meson χPT. Δ^* and δ_{Sx} introduce 2 parameters each that are, however, frozen to reproduce PDG hyperfine and flavor splittings. The total number of fit parameters is 67 (compared with 60 for the decay-constant fit [14]).

In Eq. (3.28), $\overline{m}_h$ is given self-consistently by using the formula

$$\begin{aligned}\overline{m}_h = m_{p4s,\overline{\mathrm{MS}}}(2\ \mathrm{GeV})&\left[\frac{C(\alpha_{\overline{\mathrm{MS}}}(\overline{m}_h))}{C(\alpha_{\overline{\mathrm{MS}}}(2\ \mathrm{GeV}))}\right]_{\text{Eq. (3.23)}}\left[\frac{am_{0h}}{am_{0,p4s}}\right]_{\mathrm{sim}}\times \\ &\left(1 + \alpha_{\overline{\mathrm{MS}}}(2\ \mathrm{GeV})\sum_{n=1}^{4} k_n x_h^n\right)\times\left(1 + \tilde{c}_1\alpha_s y + \tilde{c}_2 y^2 + \tilde{c}_3 y^3\right),\end{aligned} \tag{3.29}$$

to readjust the argument of $C(\alpha_{\overline{\mathrm{MS}}}(\overline{m}_h))$. These parameters are not new but the same as those in Eq. (3.28).

IV. EFT FIT TO DETERMINE THE QUARK MASSES

In Sec. III, we have constructed a function with 67 fit parameters that is motivated by EFTs. Here, we use this function to perform a correlated fit to partially-quenched data at five lattice spacings, from $a \approx 0.12$ fm to ≈ 0.03 fm, and at several values of the light sea-quark masses. A sixth lattice spacing, $a \approx 0.15$ fm, is used to check discretization errors but is not included in the base fit. At the coarsest lattice spacings, we only have data with two different values for valence heavy-quark mass: $m_h = m_c'$ and $m_h = 0.9m_c'$, where m_c' is the simulation value of sea charm-quark mass in each ensemble. It is close to but not precisely equal to the physical charm mass m_c because of tuning errors. We include data with $0.9m_c' \le m_h \le 5m_c'$ subject to condition $am_h < 0.9$, which is chosen to avoid large lattice artifacts. For every valence heavy quark, we use several light valence quarks with masses $m_l \lesssim m_x \lesssim m_s$; on ensembles with the mass of the strange sea quark close to its physical value, m_x/m_s' takes values in a subset of $\{0.036, 0.1, 0.2, 0.4, 0.6, 1.0\}$ (in several cases the whole set). In the base fit, we obtain the meson masses from fits to two-point correlators with three pseudoscalar states and two opposite-parity states, which we denote "3+2" below. To investigate the error arising from excited state contamination, we also use meson-mass data from (2+1)-state fits.

The values of the bare masses corresponding to the light and strange quarks are taken from combinations of the physical pion and kaon masses, as discussed in Refs. [14] and [50]. Similarly, the physical charmed and bottom quarks are defined so that the D_s- and B_s-meson masses take their physical values. Because the gauge-field ensembles omit electromagnetism, we need to subtract electromagnetic effects from the experimentally measured masses, which means introducing a specific scheme to do so. We identify $M_{\pi^0}^{\rm QCD} = M_{\pi^0}^{\rm expt}$ and adjust m_l accordingly. Then, m_s is tuned to obtain

$$\left(M_{K^+}^2 + M_{K^0}^2 - M_{\pi^0}^2\right)^{\rm QCD} = \left(M_{K^+}^2 + M_{K^0}^2 - M_{\pi^0}^2\right)^{\rm expt} - 2\left(M_{K^0}^2\right)^{\gamma} - (1+\epsilon')\left(M_{\pi^+}^2 - M_{\pi^0}^2\right)^{\rm expt}, \tag{4.1}$$

with $\left(M_{K^0}^2\right)^{\gamma} = 44(3)_{\rm stat}(25)_{\rm syst}$ MeV^2 and $\epsilon' = 0.74(1)_{\rm stat}(^{+8}_{-11})_{\rm syst}$ [63]. Our scheme is the one introduced for u, d quarks in Ref. [64] and extended naturally to the s quark using the fact that mass renormalization for staggered quarks is multiplicative [63]. Numerically, the scheme dependence predominantly affects $\left(M_{K^0}^2\right)^{\gamma}$ and has relatively little influence on the value of ϵ'.

As in Ref. [14], we tune m_c and m_b with the phenomenological formula [65–67]

$$M_{H_x}^{\rm expt} = M_{H_x}^{\rm QCD} + Ae_xe_h + Be_x^2, \tag{4.2}$$

where $A = 4.44$ MeV, $B = 2.4$ MeV [14] and e_x and e_h are charges of the valence light quark and heavy antiquark, respectively. Using these quantities, the quark charges, and the experimental meson masses $M_{D_s}^{\rm expt} = 1968.27(10)$ MeV and $M_{B_s}^{\rm expt} = 5366.82(22)$ MeV [52], we compute the pure QCD masses $M_{D_s}^{\rm QCD} = 1967.01$ MeV and $M_{B_s}^{\rm QCD} = 5367.04$ MeV. This choice for defining $M_{H_x}^{\rm QCD}$ amounts to a specific QED renormalization scheme for the heavy-quark mass. Another choice, for example, would be to subtract the leading QED contribution to the self-energy of the heavy quark, which is proportional to e_h^2. Finally, we set $(aM_{H_s}/af_{p4s})^{\rm sim} = M_{H_s}^{\rm QCD}/f_{p4s}$ to find the physical am_c and am_b on each ensemble.

In the one-loop χPT result, Eq. (3.2), finite-volume effects enter through the function K_1. Because the numerical evaluation of those effects is time-consuming, our base fit, as well as various alternative fits that we employ to estimate or check statistical and systematic errors,

use the infinite-volume version of K_1. The finite-volume correction is determined only in a single fit at the end of the analysis. Cross terms between finite-volume and other systematic errors are missed with this approach, but they are negligible.

We use a constrained fitting procedure [68] with priors set as follows. For the main objectives of the analysis, we choose extremely wide priors: 0 ± 6 GeV for both $m_{p4s,\overline{\rm MS}}(2\text{ GeV})$ and $\overline{\Lambda}_{\rm MRS}$, and $(0 \pm 1)\Lambda^2_{\rm HQET}$ for μ_π^2. Several other parameters are set from external considerations. As discussed in Sec. III A, the value of $\mu_G^2(m_b)$ should be close to the B^*-B hyperfine splitting; following Ref. [69], we set the prior distribution of $\mu_G^2(m_b)$ to (0.35 ± 0.07) GeV^2. For the LECs that appear at LO in HMrASχPT and are common for both decay constants and meson masses, we use the same prior constraints as in our work on decay constants [14]:

$$g_\pi \sim 0.53 \pm 0.08, \tag{4.3a}$$

$$\frac{1}{f^2} \sim \frac{1}{2}\left(\frac{1}{f_\pi^2} + \frac{1}{f_K^2}\right) \pm \left(\frac{1}{f_\pi^2} - \frac{1}{f_K^2}\right), \tag{4.3b}$$

$$\delta'_V/\bar{\Delta} \sim -0.88 \pm 0.09, \tag{4.3c}$$

$$\delta'_A/\bar{\Delta} \sim +0.46 \pm 0.23, \tag{4.3d}$$

where $a^2\bar{\Delta}$ is related to the differences in squared pion masses, as discussed in Ref. [14]. For the LECs λ_1 and λ'_1, we use wide priors of (0 ± 2) GeV^{-1}, which are 10 times larger than what can be extracted from the flavor splittings of B or D mesons, namely $\lambda_1 \approx 0.2$ GeV^{-1} (see, for example, Ref. [70]). Similarly, for the dimensionless LECs λ_{a^2} and λ'_{a^2}, we use priors of 0 ± 10, which are much wider than the expected size of order 1.

For the overall normalization of R_n, which is denoted by N_m in Ref. [22] and N in Ref. [21, 23], we use

$$R_0 = 0.535 \pm 0.010 \tag{4.4}$$

for a theory with three massless active quarks [23]. In the fits reported in this section, we use Eq. (4.4) to provide a prior for R_0.

Finally, the remaining parameters, which are dimensionless, are given the prior 0 ± 1.

The calculation of the MRS mass relies on having a precise estimate for the strong coupling. In this paper, we use

$$\alpha_{\overline{\rm MS}}(5\text{ GeV}; n_f = 4) = 0.2128(25), \tag{4.5}$$

which has been obtained by HPQCD Collaboration [71] for four active flavors. This value corresponds to $\alpha_{\overline{\rm MS}}(m_Z; n_f = 5) = 0.11822(74)$, whereas the PDG quotes $\alpha_{\overline{\rm MS}}(m_Z; n_f = 5) = 0.1181(11)$ with a somewhat larger uncertainty. The advantage of Eq. (4.5) is that it has been determined on a subset of the same ensembles used here, so it is consistent to use it with our lattice-QCD data. We use the mean value in our base fit, and we introduce an uncertainty associated with $\alpha_{\overline{\rm MS}}$ by varying its value by 1σ. To run the coupling constant to the scale μ, we use the QCD beta function at five-loop order accuracy [58] and integrate the differential equation numerically. In Sec. V, we comment on how the results would change using the PDG's estimate of the uncertainty in $\alpha_{\overline{\rm MS}}$.

In general, our data for the meson masses are more precise than the data for scale-setting quantities. We incorporate the latter uncertainties as follows. Let us use af_{p4s} and am_{p4s} to denote the $p4s$ quantities computed from light mesons at each lattice spacing and Σ_{p4s} to denote their covariance matrix. We introduce two fit parameters at each lattice spacing,

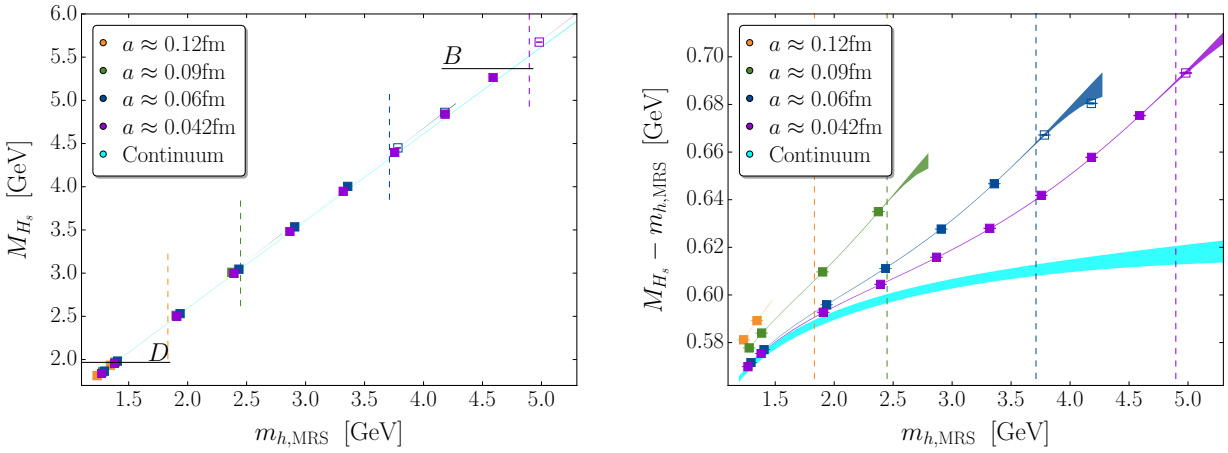

FIG. 1. A snapshot of the base fit (to data for all light-quark masses) and the lattice data for heavy-strange meson masses. Only ensembles with physical light sea mass are shown, thereby leaving out the finest lattice spacing, $a \approx 0.03$ fm. Left: heavy-strange meson mass vs. heavy-quark MRS mass. Right: difference of the heavy-strange meson mass and the heavy-quark MRS mass vs. heavy-quark MRS mass. The dashed vertical lines indicate the cut $am_h = 0.9$ for each lattice spacing. Data points with open symbols to the right of the dashed vertical lines are omitted from the fit. Here $m_{h,\mathrm{MRS}}$ is the continuum limit of the MRS mass of the heavy quark h. The error bar for $m_{h,\mathrm{MRS}}$ is suppressed for clarity.

$af_{p4s,\mathrm{opt}}$ and $am_{p4s,\mathrm{opt}}$, to represent optimized values for the $p4s$ quantities under the influence of the heavy-light data. We then employ the so-called penalty trick [72] to take into account the uncertainties in af_{p4s} and am_{p4s}. Thus, we add

$$\delta\chi^2 = \sum \left[af_{p4s} - af_{p4s,\mathrm{opt}} \quad am_{p4s} - am_{p4s,\mathrm{opt}}\right] (\Sigma_{p4s})^{-1} \begin{bmatrix} af_{p4s} - af_{p4s,\mathrm{opt}} \\ am_{p4s} - am_{p4s,\mathrm{opt}} \end{bmatrix} \tag{4.6}$$

to our χ^2 function, where the sum is over all lattice spacings. Because data at 5 different lattice spacings enter the base fit, 10 additional parameters are required. The optimized values for the scale setting quantities are then obtained simultaneously in the EFT fit. Given the size of errors in our data, the bias discussed in Ref. [72] is negligible.

Altogether we have 384 lattice data points and 77 parameters in our base fit: 67 parameters in the EFT fit function and 10 parameters for optimized values of scale-setting quantities. The fit returns a correlated $\chi^2_{\mathrm{data}}/\mathrm{dof} = 312/307$, giving a p value of $p = 0.3$. Figures 1 and 2 illustrate the base fit at the four (five) lattice spacings for the physical mass ($0.2m'_s$) ensembles and in the continuum limit. The valence light mass m_x is tuned to m_s: the graphs illustrate a snapshot for heavy-strange meson masses. We plot the heavy-strange meson mass or the difference of the meson mass and the $\bar{h}$-antiquark MRS mass versus the continuum limit of the h-quark MRS mass (in Fig. 1) or its reciprocal (in Fig. 2). Data points with open symbols to the right (left) of the dashed vertical line of the corresponding color in Fig. 1 (Fig. 2) are omitted from the fit because they have $am_h > 0.9$. In the continuum extrapolation the masses of sea quarks are set to the physical (correctly tuned) quark masses m_l, m_s and m_c, while at nonzero lattice spacing the masses of the sea quarks take their simulation values.

The width of the fit lines in Figs. 1 and 2 show the statistical error coming from the fit, which is only part of the total statistical error, since it does not include the statistical errors

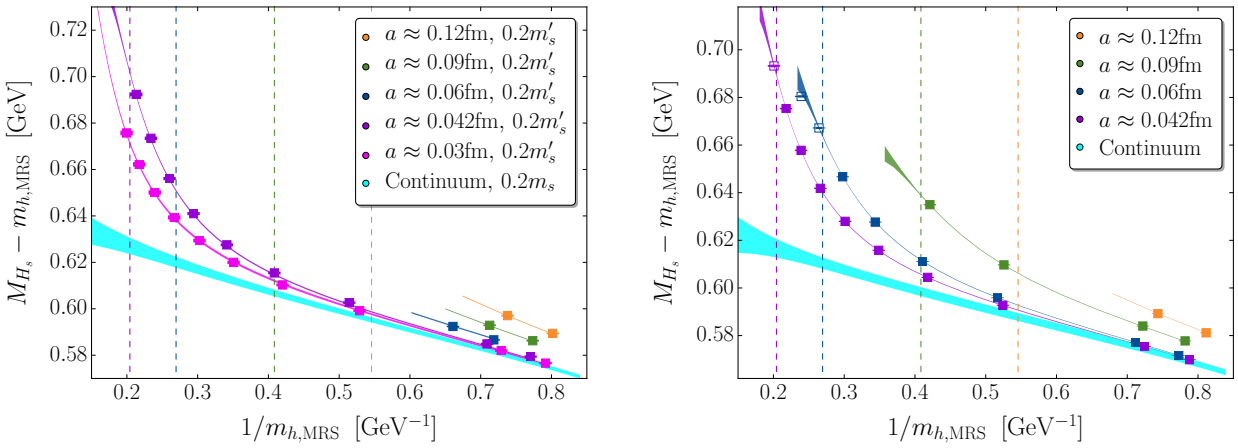

FIG. 2. Similar to Fig. 1, but the horizontal axes are the inverse of the heavy-quark MRS mass, and the left panel shows ensembles with light sea mass equal to $0.2m'_s$, while the right panel shows physical-mass ensembles. Data points with open symbols to the left of the dashed vertical lines are omitted from the fit.

in the inputs of the light quark masses and the lattice scale. Furthermore, the statistical error reported by the fit is sensitive to numerical errors in computing the fit parameters' covariance matrix. For a robust determination of the total statistical error of each output quantity, we divide the full data set into 20 jackknife resamples. The complete calculation, including the determination of the inputs, is performed on each resample, and the error is computed as usual from the variations over the resamples. For convenience, we keep the covariance matrix fixed to that of the full data set, rather than recomputing it for each resample.

The physically interesting quantities $m_{p4s,\overline{\mathrm{MS}}}(2\ \mathrm{GeV})$, $\overline{\Lambda}_{\mathrm{MRS}}$, μ_π^2, and $\mu_G^2(m_b)$ are now determined directly from the fit to the lattice data. Moreover, the fit function evaluated at zero lattice spacing and physical sea-quark masses yields the meson masses as a function of the valence heavy and light quark masses; see, *e.g.*, Figs. 1 and 2.

Figure 3 shows the stability of our final results for $\overline{\mathrm{MS}}$ quark mass ratios m_b/m_c, m_c/m_s and m_b/m_c; for masses of strange, charm and bottom quarks; and for the HQET matrix element $\overline{\Lambda}_{\mathrm{MRS}}$. We test the systematic error in the continuum extrapolation by repeating the fit after either adding in the coarsest ($a \approx 0.15$ fm) ensembles or omitting the finest ($a \approx 0.03$ fm) ensemble. These changes are shown in Fig. 3 and seen to have no significant effect, so we consider these tests to be cross-checks. The meson-mass data in our base fit are obtained from the (3+2)-state fits to two-point correlators. To investigate the error arising from excited state contamination, we repeat the EFT fit with meson-mass data from the (2+1)-state fits to two-point correlators. As seen in Fig. 3, the effects from this change are small too. Because we have no other handle on systematic errors due to excited states, we take the difference between the results from the two types of correlator fits as an estimate of this uncertainty.

We now turn to effects from truncating perturbative QCD in the relation between quark-mass definitions and the beta function. As explained with Eq. (1.3), the MRS mass connects the $\overline{\mathrm{MS}}$ mass of the h quark to the heavy-light-meson mass H_x. By design, the fit yields $m_{p4s,\overline{\mathrm{MS}}}(2\ \mathrm{GeV})$, and we use the continuum limit of am_h/am_{p4s} to convert to $m_{h,\overline{\mathrm{MS}}}(2\ \mathrm{GeV})$. We then use Eqs. (3.22) and (3.23) to calculate $\overline{m}_h$ and Eq. (3.24) to calculate $m_{h,\mathrm{MRS}}$. The

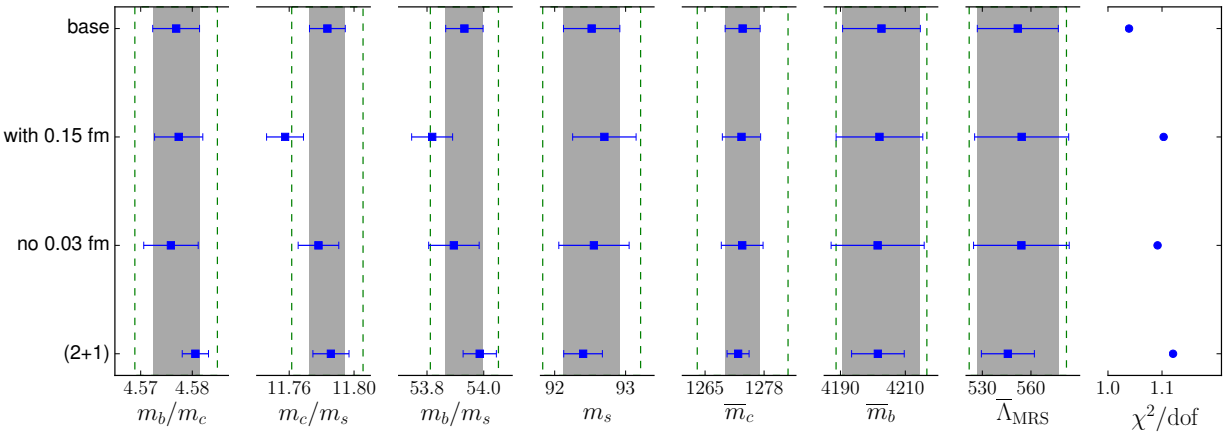

FIG. 3. Stability plot showing the sensitivity under variations in the data set and the form of the fit function, as described in the text. Here $m_s = m_{s,\overline{\rm MS}}(2\ {\rm GeV})$, $\overline{m}_c = m_{c,\overline{\rm MS}}(m_{c,\overline{\rm MS}})$, and $\overline{m}_b = m_{b,\overline{\rm MS}}(m_{b,\overline{\rm MS}})$. The error bars show only the statistical errors, the gray error bands correspond to the statistical error of the base fit, and the dashed green lines correspond to total errors.

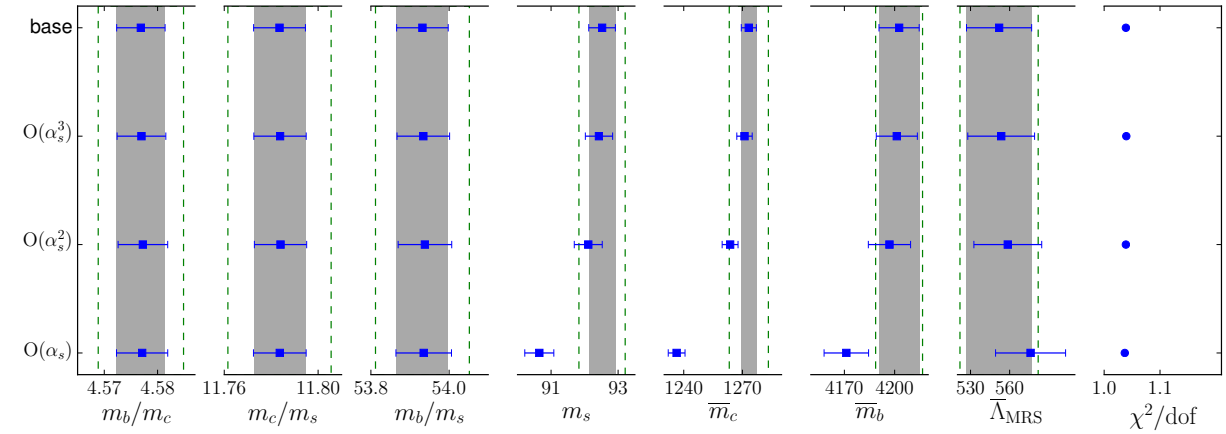

FIG. 4. Stability plot showing the sensitivity to truncation error in perturbative-QCD relations that are used in our analysis. In the base fit, the perturbative series are accurate through order α_s^4. In the fits labeled by $O(\alpha_s^n)$, we keep n subleading orders. Here $m_s = m_{s,\overline{\rm MS}}(2\ {\rm GeV})$, $\overline{m}_c = m_{c,\overline{\rm MS}}(m_{c,\overline{\rm MS}})$, and $\overline{m}_b = m_{b,\overline{\rm MS}}(m_{b,\overline{\rm MS}})$. The error bars show only the statistical errors, the gray error bands correspond to the statistical error of the base fit, and the dashed green lines correspond to total errors.

beta function and quark-mass anomalous dimension are known at five loops [57, 58], and the pole mass at four loops [59, 60].

To monitor the errors from truncating perturbative QCD, we rerun the analysis with fewer orders in Eqs. (3.23) and (3.24) and in the beta function without, however, changing $C_{\rm cm}$, the Wilson coefficient for μ_G^2, Eq. (3.7). Figure 4 shows the stability of our results for $\overline{\rm MS}$ quark mass ratios m_b/m_c, m_c/m_s and m_b/m_c; for masses of strange, charm and bottom quarks; and for the HQET matrix element $\overline{\Lambda}_{\rm MRS}$, as the order of perturbation theory is increased. In Fig. 4, we denote by $O(\alpha_s^n)$ a fit that includes n orders beyond the leading terms in Eqs. (3.23), (3.24), and the beta function. The quark mass ratios are not at all

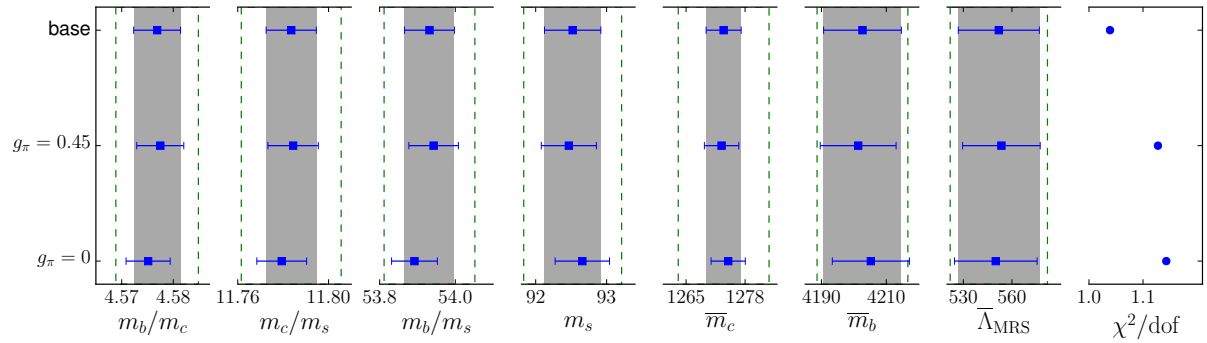

FIG. 5. Stability plot showing the sensitivity to different choices for g_π. The error bars show only the statistical errors, the gray error bands correspond to the statistical error of the base fit and the dashed green lines correspond to total errors.

sensitive to the truncations in the perturbative-QCD relations; essentially, these ratios are the continuum limit of the corresponding bare masses. For the quark masses and the HQET matrix elements, one finds good convergence, within the statistical errors, as the order of α_s in the perturbative expressions is increased. Based on this observation, we do not introduce any additional systematic error associated with truncation in perturbative-QCD results.

Our data prefer an overall coefficient of the one-loop HMrASχPT contribution, δM_{H_x}, namely g_π^2/f^2, well below the prior width of the product of g_π^2 and $1/f^2$ in Eqs. (4.3a) and (4.3b). In our base fit, the posterior for this product is $g_\pi^2/f^2 = 3.8$ GeV^{-2} (for D systems) while the prior value is (14 ± 7) GeV^{-2}. To investigate the effects of treating g_π^2 and $1/f^2$ as free parameters, we consider two alternative fits. First, we fix $g_\pi = 0.45$, one sigma below its nominal value, and $1/f^2 = 1/f_K^2$. Second, we fix $g_\pi = 0$, which is equivalent to fitting to a polynomial in the quark masses. In Fig. 5, we label the first of these "$g_\pi = 0.45$" and the second "$g_\pi = 0$". As one can see, the quark-mass ratios, quark masses themselves, and the HQET matrix element $\overline{\Lambda}_{\rm MRS}$ do not change significantly under these variations. Consequently, we do not introduce any additional systematic error associated with our treatment of g_π and $1/f^2$.

Our full error budget for quark-mass ratios, quark masses, and the HQET matrix element $\overline{\Lambda}_{\rm MRS}$ is given in Table I. The row labeled "statistics and EFT fit" lists the uncertainty reported by the Bayesian fit, which incorporates associated systematic effects of extrapolation. There are further systematic effects not captured in the EFT fit. The excited-state contamination in two-point correlator fits is explained above. Our method of estimating the systematic error associated with the tuned quark masses and scale setting quantities is similar to that in Ref. [14]. We correct for (exponentially small) finite-volume effects using the finite-volume version of the NLO χPT for the heavy-light mesons, and using NLO or NNLO χPT for the light-quark and scale-setting inputs following Ref. [50]. Residual finite-volume effects from higher orders in χPT are estimated, as in Ref. [14], as 0.3 times the calculated finite-volume correction. The nonequilibration of topological charge in our finest ensembles causes small finite-volume effects that are not exponentially suppressed [73]. Although this error is negligible for masses of heavy-light mesons, even with our high statistics, we include the shift expected from Ref. [73] as a systematic error. Note that, despite the fact that we take the full topological shift as the associated error, these errors all round to zero at the precision shown in Table I. The uncertainties stemming from the omission of electro-

TABLE I. Error budget for strange-, charm- and bottom-quark masses, their ratios, and the HQET matrix element $\overline{\Lambda}_{\rm MRS}$. See the text for the description.

Error (%)	m_b/m_c	m_c/m_s	m_b/m_s	$m_{s,\overline{\rm MS}}(2\ {\rm GeV})$	$\overline{m}_c$	$\overline{m}_b$	$\overline{\Lambda}_{\rm MRS}$
Statistics and EFT fit	0.10	0.09	0.12	0.43	0.30	0.29	4.5
Two-point correlator fits	0.08	0.02	0.10	0.13	0.08	0.03	1.1
Scale setting and tuning	0.02	0.08	0.10	0.12	0.03	0.02	0.2
Finite-volume corrections	0.02	0.04	0.06	0.07	0.02	0.01	0.1
Topological charge distribution	0.00	0.00	0.00	0.00	0.00	0.00	0.0
Electromagnetic corrections	0.11	0.11	0.01	0.02	0.08	0.01	0.1
α_s	0.01	0.00	0.01	0.56	0.75	0.18	2.9
$f_{\pi,\rm PDG}$	0.03	0.07	0.10	0.13	0.04	0.02	0.3

TABLE II. Error contributions from electromagnetic effects to strange-, charm- and bottom-quark masses, their ratios, and the HQET matrix element $\overline{\Lambda}_{\rm MRS}$. The sources of uncertainty are described in the text.

Error (%)	m_b/m_c	m_c/m_s	m_b/m_s	$m_{s,\overline{\rm MS}}(2\ {\rm GeV})$	$\overline{m}_c$	$\overline{m}_b$	$\overline{\Lambda}_{\rm MRS}$
K^+-K^0 splitting	+0.00	+0.01	+0.01	−0.01	−0.00	−0.00	+0.0
K^0 mass	+0.00	+0.00	+0.01	−0.01	−0.01	−0.01	+0.1
H_x mass	−0.11	+0.11	−0.00	−0.01	+0.07	−0.01	+0.0

magnetism are discussed in detail below. Finally, our results have uncertainties from the parametric inputs α_s, given in Eq. (4.5), and $f_{\pi,\rm PDG} = 130.50(13)$ MeV [52].

Table II shows a breakdown of the uncertainties from matching a pure-QCD calculation such as this to QCD+QED. Briefly, "K^+-K^0 splitting" is the uncertainty in connecting the K^+-K^0 splitting to that of π^+-π^0, stemming from ϵ', and "K^0 mass" refers to the uncertainty in the electromagnetic contribution to the neutral kaon mass, $\left(M^2_{K^0}\right)^\gamma$. These two effects are negligible compared with the other sources of uncertainty. In this work, we choose a specific scheme [63, 64] for the electromagnetic contribution to the neutral kaon masses; other works, for example the FLAG report [74], choose other schemes. Changing $\left(M^2_{K^0}\right)^\gamma$ from +44 MeV^2 to +461 MeV^2 reduces m_s by 0.17% and, consequently, increases m_c/m_s and m_b/m_s by 0.17%. When using these ratios and the strange-quark mass in a setting that ignores the subtleties of the QED scheme, one may wish to incorporate an additional uncertainty of ±0.17%.

Another uncertainty comes from the estimates of the electromagnetic correction to the heavy-light meson mass, described above with Eq. (4.2). It is denoted "H_x mass" in Table II. For the associated error, we take the difference between results obtained with and without the electromagnetic shift. Results for heavy-quark masses depend on the chosen QED quark-mass scheme. As discussed above, we do not subtract any part of the QED self-energy. [Equation (4.2) contains no term proportional to e_h^2.] When using other schemes, one should convert our results accordingly: a shift of 1 MeV in the QCD part of the D_s (B_s) mass leads to a 0.83 MeV (1 MeV) shift in $\overline{m}_c$ ($\overline{m}_b$). The scheme dependence on the meson masses may be estimated as $\pm\alpha m_h e_h^2 \approx \pm 4.2$ MeV (average for D_s and B_s). When using the heavy-quark masses in a setting that ignores the subtleties of the QED scheme, one may consequently

wish to incorporate an additional uncertainty of ± 3.5 MeV on $\overline{m}_c$ and ± 4.2 MeV on m_b.

V. RESULTS

In this section, we collect the results that stem from the EFT fits described in the previous two sections. These fall into four categories: quark masses themselves and their ratios, HQET matrix elements, flavor splittings in the D and B systems, and LECs of HMχPT. We emphasize again that our final results for quark masses depend on our prescription for calculating QCD-only meson masses; cf. the discussions around Eq. (4.2) and about Table II.

A. Quark Masses

As discussed in Sec. IV, the main physical fit parameters correspond to the terms in Eq. (1.1). For the masses, the fit yields

$$m_{p4s,\overline{\rm MS}}(2\ {\rm GeV}) = 37.01(16)_{\rm stat}(07)_{\rm syst}(21)_{\alpha_s}(05)_{f_{\pi,\rm PDG}}\ {\rm MeV} \tag{5.1}$$

with four active flavors, from which it follows immediately

$$m_{s,\overline{\rm MS}}(2\ {\rm GeV}) = 92.52(40)_{\rm stat}(18)_{\rm syst}(52)_{\alpha_s}(12)_{f_{\pi,\rm PDG}}\ {\rm MeV}. \tag{5.2}$$

Having determined the strange quark mass, we use the quark mass ratios m_s/m_l and m_u/m_d, and their correlations, to obtain the light quark masses

$$m_{l,\overline{\rm MS}}(2\ {\rm GeV}) = 3.404(14)_{\rm stat}(08)_{\rm syst}(19)_{\alpha_s}(04)_{f_{\pi,\rm PDG}}\ {\rm MeV}, \tag{5.3}$$
$$m_{u,\overline{\rm MS}}(2\ {\rm GeV}) = 2.118(17)_{\rm stat}(32)_{\rm syst}(12)_{\alpha_s}(03)_{f_{\pi,\rm PDG}}\ {\rm MeV}, \tag{5.4}$$
$$m_{d,\overline{\rm MS}}(2\ {\rm GeV}) = 4.690(30)_{\rm stat}(36)_{\rm syst}(26)_{\alpha_s}(06)_{f_{\pi,\rm PDG}}\ {\rm MeV}, \tag{5.5}$$

where m_l is again the average of the up- and down-quark masses. To obtain these results, we use a slightly different uncertainty for the ratios than those reported in Ref. [14]. Here, $m_s/m_l = 27.182(46)_{\rm stat}(56)_{\rm syst}(1)_{f_{\pi,\rm PDG}}$ and $m_u/m_d = 0.4517(55)_{\rm stat}(101)_{\rm syst}(0)_{f_{\pi,\rm PDG}}$. The systematic error omits (for consistency) the contribution from the K^0-mass scheme and takes the larger side of the asymmetric uncertainty from the choice of continuum extrapolation.

Evaluating the fit function at the quark masses yielding the D_s and B_s mesons yields the mass ratios

$$m_c/m_s = 11.784(11)_{\rm stat}(17)_{\rm syst}(00)_{\alpha_s}(08)_{f_{\pi,\rm PDG}}, \tag{5.6}$$
$$m_b/m_s = 53.93(7)_{\rm stat}(8)_{\rm syst}(1)_{\alpha_s}(5)_{f_{\pi,\rm PDG}}, \tag{5.7}$$
$$m_b/m_c = 4.577(5)_{\rm stat}(7)_{\rm syst}(0)_{\alpha_s}(1)_{f_{\pi,\rm PDG}} \tag{5.8}$$

where the third line is the ratio of the first two, taking correlations in the uncertainties into account. In m_c/m_s and m_b/m_c, the uncertainty stemming from α_s rounds to zero. As elsewhere in this paper, these quark-mass ratios are given in our scheme for subtracting electromagnetic contributions from the K^0, D_s, and B_s meson masses. With this proviso in mind, though, they hold for any mass-independent renormalization scheme of QCD.

For the charm- and bottom-quark masses we then obtain

$$m_{c,\overline{\rm MS}}(2\ {\rm GeV}) = 1090(5)_{\rm stat}(2)_{\rm syst}(6)_{\alpha_s}(1)_{f_{\pi,\rm PDG}}\ {\rm MeV}, \tag{5.9}$$

$$m_{b,\overline{\rm MS}}(2\ {\rm GeV}) = 4990(17)_{\rm stat}(2)_{\rm syst}(29)_{\alpha_s}(1)_{f_{\pi,\rm PDG}}\ {\rm MeV}, \tag{5.10}$$

again for four active flavors. The relative systematic error is larger for $m_{c,\overline{\rm MS}}(2\ {\rm GeV})$ than for $m_{b,\overline{\rm MS}}(2\ {\rm GeV})$, because much of it comes from additive parts of the two-point correlator and electromagnetic uncertainties. The largest uncertainty comes from the uncertainty in α_s in Eq. (4.5), followed by the statistical error (after propagation through the EFT fit). As one can see from Fig. 4 and Eq. (5.18), below, this uncertainty does not come from order-by-order changes in perturbative QCD: the α_s uncertainty is parametric.

The uncertainty stemming from α_s becomes smaller at higher renormalization points. For the charmed quark,

$$m_{c,\overline{\rm MS}}(3\ {\rm GeV}) = 984.3(4.2)_{\rm stat}(1.6)_{\rm syst}(3.2)_{\alpha_s}(0.6)_{f_{\pi,\rm PDG}}\ {\rm MeV}, \tag{5.11}$$

or, adding all errors in quadrature, 984.3(5.6) MeV. Running from one renormalization scale is carried out with Eq. (3.23) and numerical integration of the differential equation for $\alpha_{\overline{\rm MS}}$ with the five-loop beta function. For comparison to the literature (cf. Sec. VI), it is useful to have $\overline{m}_h = m_{h,\overline{\rm MS}}(m_{h,\overline{\rm MS}})$; for charm and bottom

$$\overline{m}_c = 1273(4)_{\rm stat}(1)_{\rm syst}(10)_{\alpha_s}(1)_{f_{\pi,\rm PDG}}\ {\rm MeV}, \tag{5.12}$$

$$\overline{m}_b = 4203(12)_{\rm stat}(1)_{\rm syst}(8)_{\alpha_s}(1)_{f_{\pi,\rm PDG}}\ {\rm MeV}, \tag{5.13}$$

or, adding all errors in quadrature, $\overline{m}_c = 1273(10)$ MeV and $\overline{m}_b = 4203(14)$ MeV.

The quark masses given above are for four active flavors. The mass of the bottom quark with five active flavors can be calculated from [75]

$$m_b^{(n_l)}(\mu) = {\overline{m}_b}^{(n_f)}\left[1 + 0.2060\left(\frac{\alpha_s^{(n_f)}(\mu)}{\pi}\right)^2 + (1.8476 + 0.0247 n_l)\left(\frac{\alpha_s^{(n_f)}(\mu)}{\pi}\right)^3 \right.$$
$$\left. +(6.850 - 1.466 n_l + 0.05616 n_l^2)\left(\frac{\alpha_s^{(n_f)}(\mu)}{\pi}\right)^4 + \cdots\right], \tag{5.14}$$

where $n_l = n_f - 1$ and $\mu = {\overline{m}_b}^{(n_f)}$. Setting $n_f = 5$, we obtain

$$\overline{m}_b^{(n_f=5)} = 4197(12)_{\rm stat}(1)_{\rm syst}(8)_{\alpha_s}(1)_{f_{\pi,\rm PDG}}\ {\rm MeV}, \tag{5.15}$$

or, adding all errors in quadrature, $\overline{m}_b = 4197(14)$ MeV. The five-flavor mass can be run from $\overline{m}_b^{(n_f=5)}$ to higher scales using the five-loop anomalous dimension [57] and beta function [58] with $n_f = 5$.

Using the above results and Eqs. (1.3a) and (3.24), we obtain the charm and bottom masses in the MRS scheme:

$$m_{c,\rm MRS} = 1393(6)_{\rm stat}(9)_{\rm syst}(6)_{\alpha_s}(0)_{f_{\pi,\rm PDG}}\ {\rm MeV}, \tag{5.16}$$

$$m_{b,\rm MRS} = 4751(13)_{\rm stat}(4)_{\rm syst}(11)_{\alpha_s}(1)_{f_{\pi,\rm PDG}}\ {\rm MeV}, \tag{5.17}$$

or, adding all errors in quadrature, $m_{c,\rm MRS} = 1393(13)$ MeV and $m_{b,\rm MRS} = 4751(18)$ MeV. Similar to the stability shown in Fig. 4, the ratio $m_{\rm MRS}/\overline{m}$ is very stable. For $\alpha_s = 0.22$ and three flavors of massless quarks,

$$m_{\rm MRS}/\overline{m} = (1.133, 1.131, 1.132, 1.132) \tag{5.18}$$

at one through four loops, while

$$m_{\rm pole}/\overline{m} = (1.093, 1.143, 1.183, 1.224), \tag{5.19}$$

omitting in both cases the charm sea-quark contribution $\Delta m_{(c)}$ for simplicity.

If we use the PDG's estimate of the uncertainty in $\alpha_{\overline{\rm MS}}$ instead of that in Eq. (4.5), then each uncertainty associated with α_s increases by about 50%, namely to 0.77 MeV, 0.039 MeV, and 0.018 MeV, for the strange-, down-, and up-quark masses; 4.8 MeV and 14 MeV for $m_{c,\overline{\rm MS}}(3\ {\rm GeV})$ and $\overline{m}_c$; and 11 MeV for $\overline{m}_b$.

B. HQET Matrix Elements

The EFT fit directly yields results for the HQET matrix elements. With the minimal renormalon subtraction, our result

$$\overline{\Lambda}_{\rm MRS} = 552(25)_{\rm stat}(6)_{\rm syst}(16)_{\alpha_s}(2)_{f_{\pi,\rm PDG}}\ {\rm MeV}, \tag{5.20}$$

is renormalon-free. This value corresponds to light valence mass $\frac{1}{2}(m_u + m_d)$. The kinetic and chromomagnetic matrix elements are

$$\mu_\pi^2 = 0.06(16)_{\rm stat}(14)_{\rm syst}(06)_{\alpha_s}(00)_{f_{\pi,\rm PDG}}\ {\rm GeV}^2, \tag{5.21}$$

$$\mu_G^2(m_b) = 0.38(01)_{\rm stat}(01)_{\rm syst}(00)_{\alpha_s}(00)_{f_{\pi,\rm PDG}}\ {\rm GeV}^2. \tag{5.22}$$

This value for $\mu_G^2(m_b)$ cannot be considered as a pure lattice-QCD determination because, as discussed in Sec. III A, the prior for $\mu_G^2(m_b) \sim 0.35(7)\ {\rm GeV}^2$ comes from the B-meson hyperfine splitting. The definition of μ_π^2 used here still has a renormalon ambiguity of order $\Lambda_{\rm QCD}^2$, although it is expected to be small [1, 76]. In any case, the result in Eq. (5.21) cannot be directly compared with results in the "kinetic" scheme [77, 78], where $\mu_\pi^2 \approx \mu_G^2$ is expected [79] and roughly holds [12, 80]. We checked whether our χ^2 function could be consistent with such an outcome by starting the fit at $\mu_\pi^2 = 0.35\ {\rm MeV}^2$, but found the same minimum as in Eq. (5.21). We also have tried changing the prior for μ_π^2 from $(0 \pm 0.36)\ {\rm GeV}^2$ to $(0.35 \pm 0.36)\ {\rm GeV}^2$, in which case χ^2 is minimized for $\mu_\pi^2 = 0.09(16)\ {\rm GeV}^2$ and $\mu_G^2(m_b) = 0.39(1)\ {\rm GeV}^2$, where the errors are statistical only here.

To compare Eq. (5.20) with the RS scheme at a given factorization scale ν_f, one can use [1]

$$\overline{\Lambda}_{\rm RS}(\nu_f) = \overline{\Lambda}_{\rm MRS} + \mathcal{J}_{\rm MRS}(\nu_f), \tag{5.23}$$

with the function $\mathcal{J}_{\rm MRS}$ given in Eq. (2.37) of Ref. [1]. Setting $\nu_f = 1$ GeV, we find

$$\overline{\Lambda}_{\rm RS}(1\ {\rm GeV}) = 636(25)_{\rm stat}(6)_{\rm syst}(24)_{\alpha_s}(2)_{f_{\pi,\rm PDG}}\ {\rm MeV}. \tag{5.24}$$

The uncertainty associated with α_s is larger here than for $\overline{\Lambda}_{\rm MRS}$, because $\mathcal{J}_{\rm MRS}(\nu_f)$ in Eq. (5.23) depends on $\alpha_s(\nu_f)$. Our result for $\overline{\Lambda}_{\rm RS}(1\ {\rm GeV})$ agrees with $\overline{\Lambda}_{\rm RS}(1\ {\rm GeV}) = 659$ MeV (no error quoted) [22] and 623 MeV (after rough conversion of a result in the "RS′" scheme) [81], which are obtained from the B-meson mass and the RS mass for the bottom quark.

For future phenomenological studies, Table III in the Appendix provides the correlation matrix of the MRS masses of the charm and bottom quarks with the HQET matrix elements $\overline{\Lambda}_{\rm MRS}$, μ_π^2 and $\mu_G^2(m_b)$.

C. Flavor splittings

We use the D_s- and B_s-meson masses as experimental input to set the c- and b-quark masses. Comparing the output of the fit at $m_x = m_d$ with $m_x = m_s$, we obtain the flavor splittings

$$M_{D_s} - M_{D^+} = 97.9(0.2)_{\rm stat}(0.1)_{\rm syst}(0.0)_{\alpha_s}(0.1)_{f_{\pi,\rm PDG}}(0.5)_{g_\pi}\ \text{MeV}, \tag{5.25}$$
$$M_{B_s} - M_{B^0} = 87.1(0.4)_{\rm stat}(1.3)_{\rm syst}(0.0)_{\alpha_s}(0.1)_{f_{\pi,\rm PDG}}(0.4)_{g_\pi}\ \text{MeV}. \tag{5.26}$$

These results agree with the experimental values [52]

$$(M_{D_s} - M_{D^+})^{\rm expt} = 98.69(5)\ \text{MeV}, \tag{5.27}$$
$$(M_{B_s} - M_{B^0})^{\rm expt} = 87.3(2)\ \text{MeV}. \tag{5.28}$$

In these combinations of meson masses, the leading-order electromagnetic contributions cancel. The last uncertainty here stems from the significant changes found in the alternate fits with g_π fixed to 0.45 or to 0 (the polynomial fit).

In a similar vein, we can set the quark masses to $m_x = m_l' = m_s' = 0$ to obtain the SU(3) chiral limit of charmed and b-flavored mesons, or set $m_x = m_l' = 0$ and leave $m_s' = m_s$ to obtain the SU(2) chiral limit. The results are

$$M_D^{\rm SU(3)} = 1843.1(2.2)_{\rm stat}(1.4)_{\rm syst}(0.1)_{\alpha_s}(0.1)_{f_{\pi,\rm PDG}}(1.8)_{g_\pi}\ \text{MeV} \tag{5.29}$$
$$M_D^{\rm SU(2)} = 1862.4(0.2)_{\rm stat}(1.3)_{\rm syst}(0.0)_{\alpha_s}(0.1)_{f_{\pi,\rm PDG}}(0.2)_{g_\pi}\ \text{MeV} \tag{5.30}$$

for the D system, and

$$M_B^{\rm SU(3)} = 5245.5(3.2)_{\rm stat}(2.9)_{\rm syst}(0.1)_{\alpha_s}(0.2)_{f_{\pi,\rm PDG}}(3.7)_{g_\pi}\ \text{MeV} \tag{5.31}$$
$$M_B^{\rm SU(2)} = 5273.0(0.5)_{\rm stat}(1.6)_{\rm syst}(0.0)_{\alpha_s}(0.1)_{f_{\pi,\rm PDG}}(0.5)_{g_\pi}\ \text{MeV} \tag{5.32}$$

for the B system. This information can be combined with Table XII of Ref. [14], to derive decay constants from the values of $\Phi = \sqrt{M} f$ tabulated there.

D. Low-energy Constants in HMχPT

Reference [73] uses the LECs λ_1 and λ_1' obtained in this work. In particular, the values used are those for D mesons, which come from the simple, polynomial analysis without chiral expressions, *i.e.*, $g_\pi = 0$:

$$\breve{\lambda}_{1,D} = 0.218(2)\ \text{GeV}^{-1}, \tag{5.33}$$
$$\breve{\lambda}'_{1,D} = 0.037(13)\ \text{GeV}^{-1}, \tag{5.34}$$

where the errors are statistical only, which suffices for Ref. [73]. Here, the breve is a reminder that finite-mass corrections to the LECs in the HMχPT Lagrangian are included. From the experimental data for the flavor splittings of D mesons, one finds $\breve{\lambda}_1 \approx 0.2\ \text{GeV}^{-1}$ [70].

VI. SUMMARY, COMPARISONS, AND OUTLOOK

The results presented in Sec. V show that the new HQET-based method, developed here and in Ref. [1], is both qualitatively and quantitatively successful. The qualitative success relies on the clean separation of scales provided by HQET with the MRS definition of the heavy-quark mass, while the quantitative success relies on the high statistics of the MILC Collaboration's HISQ ensembles [25–27], all 24 of which have been employed here. Also relevant to the success of the method is the availability of the order-α_s^5 perturbation theory for the running of the quark mass [57] and strong coupling [58], and the order-α_s^4 coefficient linking the $\overline{\rm MS}$ mass to the pole mass and, hence, the MRS mass [59, 60]. These features are not (yet) shared by other determinations of quark masses using lattice QCD. Although the HQET method separates the heavy-quark scale from the QCD scale, mass ratios determined in the course of this work and Ref. [14] yield results for all quarks except the top quark.

Our results for heavy-quark masses $\overline{m}_c$ and $\overline{m}_b$ are compared with other results in the literature in Fig. 6. Both panels show the most recent lattice-QCD calculation with a complete error budget from each combination of method and collaboration. For nonlattice calculations, we also show the most recent result from each method and-or collaboration, but include only those with perturbative-QCD accuracy of order-α_s^3 matching and, if needed, order-α_s^4 running.[5] As noted in Sec. V, the parametric uncertainty in α_s is one of our largest

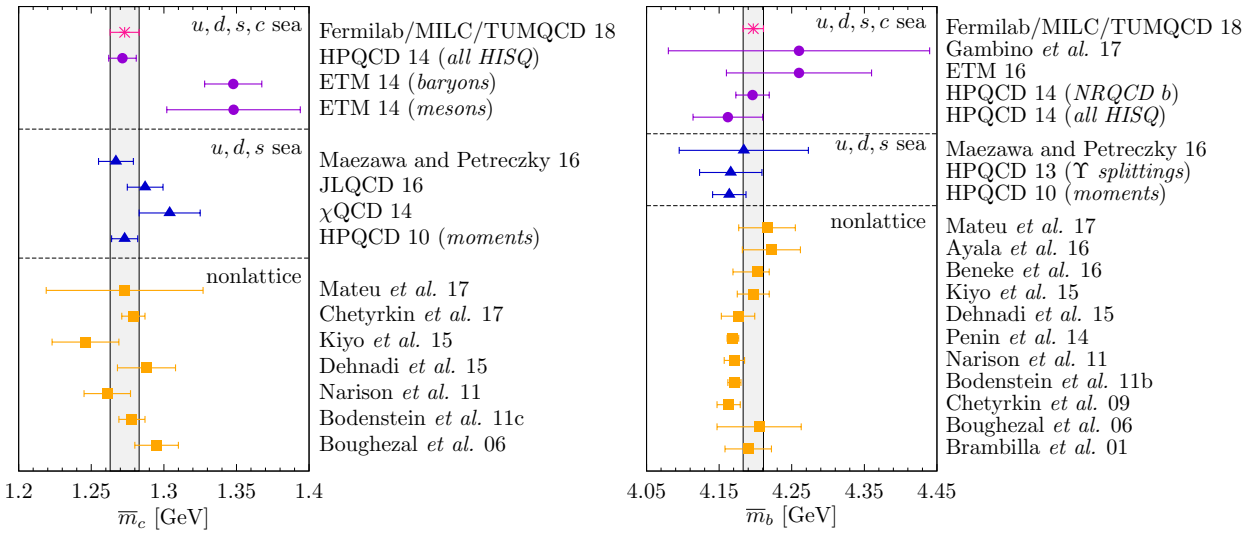

FIG. 6. Comparison of $\overline{m}_c$ (left) and $\overline{m}_b$ (right) to other results from lattice QCD and from nonlattice methods. Our result is shown as a magenta burst, with the gray band showing how it compares directly with the other results. The labels refer to Fermilab/MILC/TUMQCD 18 (this work); HPQCD 14 (*all HISQ*) [71]; ETM 14 (*baryons*) [82]; ETM 14 (*mesons*) [83]; Maezawa and Petreczky 16 [84]; JLQCD 16 [85]; χQCD 14 [86]; HPQCD 10 (*moments*) [87]; Mateu *et al.* 17 [88]; Chetyrkin *et al.* 17 [89]; Kiyo *et al.* 15 [90]; Dehnadi *et al.* 15 [91]; Narison 11 [92]; Bodenstein *et al.* 11c [93]; Boughezal *et al.* 06 [94]; Gambino *et al.* 17 [12]; ETM 16 [95]; HPQCD 14 (*NRQCD b*) [96]; HPQCD 13 (Υ *splittings*) [97]; HPQCD 10 (*moments*) [87]; Ayala *et al.* 16 [98]; Beneke *et al.* 16 [99]; Penin *et al.* 14 [100]; Bodenstein *et al.* 11b [101]; Chetyrkin *et al.* 09 [102]; Brambilla *et al.* 01 [103].

[5] If we have omitted a result with order-α_s^4 running and order-α_s^3 matching, please let us know.

uncertainties, but, thanks to the MRS mass, higher-order perturbative corrections are likely to be negligible compared with this and our statistical uncertainty; cf. Fig. 4 and Eq. (5.18).

For $\overline{m}_c$, the overall agreement is very good, and our result's uncertainty is about the same as those from charmonium correlators and (continuum) perturbative QCD, using either lattice [71] or experimental [89, 93] data as input. (References [89] and [93] differ in the moments used.) The difference between our result for $m_{c,\overline{\text{MS}}}(3\text{ GeV})$ and the recent update from Chetyrkin *et al.* [89] is 0.9σ. For $\overline{m}_b$, the overall agreement is good. The difference between our result and those of Narison [92], Bodenstein *et al.* [101], Chetyrkin *et al.* [102], and Penin and Zerf [100] is 1.3σ, 1.6σ, 1.6σ, 1.7σ, respectively. Such discrepancies among 19 independent results, especially given the importance of systematic uncertainties in all determinations, should not be seen as alarming.

It is noteworthy that for $\overline{m}_c = m_{c,\overline{\text{MS}}}(m_{c,\overline{\text{MS}}})$ the result of Ref. [89] is more precise than ours, while for $m_{c,\overline{\text{MS}}}(3\text{ GeV})$ ours is more precise. In both cases, the error bar runs as dictated by the quark-mass anomalous dimension and beta function. In addition, the order-α_s coefficient is proportional to $[\ln(3\text{ GeV}/\mu) + c]$. For the relation between $\overline{m}$ and m_{MRS}, $c > 0$, so the first-order α_s error vanishes for some $\mu > 3$ GeV. On the other hand, for the relation between $\overline{m}$ and moments of the charmonium correlator, $c < 0$, so the first-order α_s error vanishes for some $\mu < 3$ GeV. We therefore also provide light, strange, and charm masses at 3 GeV:

$$m_{l,\overline{\text{MS}}}(3\text{ GeV}) = 3.073(13)_{\text{stat}}(07)_{\text{syst}}(10)_{\alpha_s}(04)_{f_\pi,\text{PDG}}\text{ MeV}, \tag{6.1}$$

$$m_{u,\overline{\text{MS}}}(3\text{ GeV}) = 1.912(16)_{\text{stat}}(29)_{\text{syst}}(06)_{\alpha_s}(03)_{f_\pi,\text{PDG}}\text{ MeV}, \tag{6.2}$$

$$m_{d,\overline{\text{MS}}}(3\text{ GeV}) = 4.234(27)_{\text{stat}}(32)_{\text{syst}}(14)_{\alpha_s}(05)_{f_\pi,\text{PDG}}\text{ MeV}, \tag{6.3}$$

$$m_{s,\overline{\text{MS}}}(3\text{ GeV}) = 83.53(36)_{\text{stat}}(16)_{\text{syst}}(27)_{\alpha_s}(11)_{f_\pi,\text{PDG}}\text{ MeV}, \tag{6.4}$$

$$m_{c,\overline{\text{MS}}}(3\text{ GeV}) = 984.3(4.2)_{\text{stat}}(1.6)_{\text{syst}}(3.2)_{\alpha_s}(0.6)_{f_\pi,\text{PDG}}\text{ MeV}. \tag{6.5}$$

In contexts beyond the Standard Model, one needs the masses—that is the Yukawa coupling to the Higgs field—at scales of 100 GeV or higher. Table IV in the Appendix provides the correlation matrix for our charm-quark mass at 3 GeV and quark-mass ratios.

Our results for light-quark masses are compared with other results from lattice QCD in Fig. 7. As above, both panels show the most recent lattice-QCD calculations with a complete error budget from each combination of method and collaboration. As can be seen from the plots, and similar comparisons of m_u and m_d, ours are the most precise results to date. Here the precision stems from very precise quark-mass ratios from the pseudoscalar meson spectrum, together with the overall scale of quark masses from the EFT fit. Consequently, the results inherit an uncertainty due to α_s, which is largest except in the cases of $m_{d,\overline{\text{MS}}}(2\text{ GeV})$ and $m_{u,\overline{\text{MS}}}(2\text{ GeV})$, which have larger statistical and electromagnetic systematic uncertainties from m_u/m_d.

As compelling as these results are, they could be improved in several ways. First, because the EFT fit controls systematics, the statistical error (after propagation through the fit) is often the second-largest source of uncertainty, so, as usual, having more data would reduce the error. The additional data need not be more precise per se: the right panel of Fig. 2 suggests that finer lattice spacings will be needed. Second, because the other dominant uncertainty is the parametric error of α_s, it would be interesting to carry out a simultaneous determination of α_s and the quark masses, for example in a combined analysis of heavy-light meson masses and quarkonium correlators. Such an analysis would output $\overline{m}_c$, $\overline{m}_b$, and α_s *with their correlations*, which would be very convenient for determining Higgs-boson

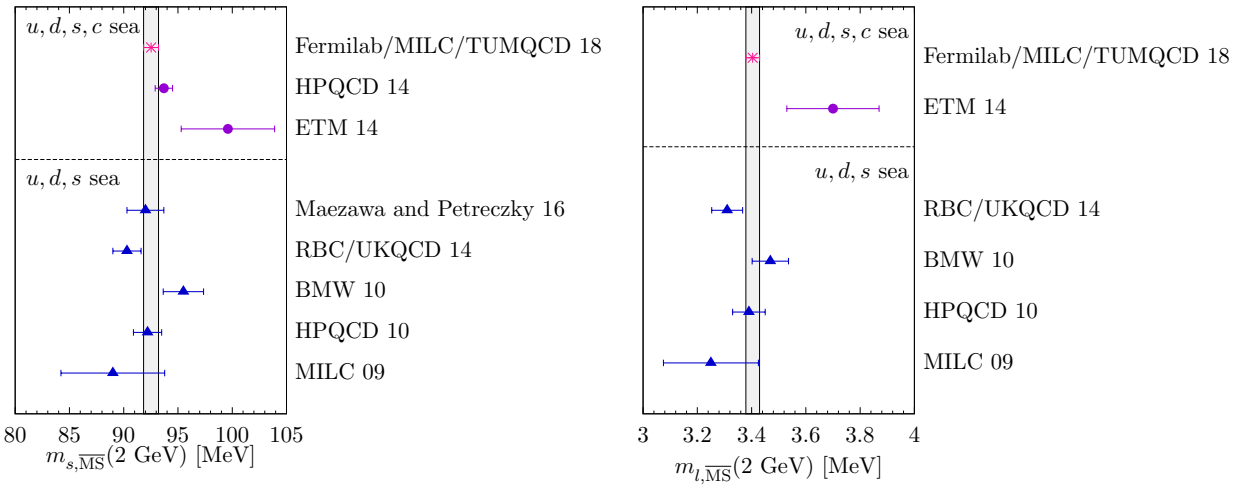

FIG. 7. Comparison of $m_{s,\overline{\rm MS}}(2\ {\rm GeV})$ (left) and $m_{ud,\overline{\rm MS}}(2\ {\rm GeV})$ (right) to other results from lattice QCD. Our result is shown as a magenta burst, with the gray band showing how it compares directly with the other results. The labels refer to Fermilab/MILC/TUMQCD 18 (this work); HPQCD 14 [71]; ETM 14 [83]; Maezawa and Petreczky 16 [84]; RBC/UKQCD 14 [104]; BMW 10 [105]; HPQCD 10 [87]; MILC 09 [106].

branching ratio in the Standard Model and extensions thereof. Third, QCD+QED simulations would eliminate the scheme dependence arising from the matching of QCD+QED to pure QCD. Finally, the ideal determination of the matrix elements μ_π^2 and μ_G^2, and analogous quantities that enter at order $1/m_Q^2$ and higher, would require computing heavy-light vector mesons on the lattice, in addition to the pseudoscalar mesons studied here. In particular, this would make possible a pure lattice result for μ_G^2, without making use of the experimental information on the B-meson hyperfine splitting.

ACKNOWLEDGMENTS

J.K. thanks Jaume Tarrús Castellà for a useful discussion on nonanalytic terms in χPT.

Computations for this work were carried out with resources provided by the USQCD Collaboration, the National Energy Research Scientific Computing Center, the Argonne Leadership Computing Facility, the Blue Waters sustained-petascale computing project, the National Institute for Computational Science, the National Center for Atmospheric Research, the Texas Advanced Computing Center, and Big Red II+ at Indiana University. USQCD resources are acquired and operated thanks to funding from the Office of Science of the U.S. Department of Energy. The National Energy Research Scientific Computing Center is a DOE Office of Science User Facility supported by the Office of Science of the U.S. Department of Energy under Contract No. DE-AC02-05CH11231. An award of computer time was provided by the Innovative and Novel Computational Impact on Theory and Experiment (INCITE) program. This research used resources of the Argonne Leadership Computing Facility, which is a DOE Office of Science User Facility supported under Contract DE-AC02-06CH11357. The Blue Waters sustained-petascale computing project is supported by the National Science Foundation (awards OCI-0725070 and ACI-1238993) and the State of Illinois. Blue Waters is a joint effort of the University of Illinois at Urbana-Champaign

and its National Center for Supercomputing Applications. This work is also part of the "Lattice QCD on Blue Waters" and "High Energy Physics on Blue Waters" PRAC allocations supported by the National Science Foundation (award numbers 0832315 and 1615006). This work used the Extreme Science and Engineering Discovery Environment (XSEDE), which is supported by National Science Foundation grant number ACI-1548562 [107]. Allocations under the Teragrid and XSEDE programs included resources at the National Institute for Computational Sciences (NICS) at the Oak Ridge National Laboratory Computer Center, the Texas Advanced Computing Center and the National Center for Atmospheric Research, all under NSF teragrid allocation TG-MCA93S002. Computer time at the National Center for Atmospheric Research was provided by NSF MRI Grant CNS-0421498, NSF MRI Grant CNS-0420873, NSF MRI Grant CNS-0420985, NSF sponsorship of the National Center for Atmospheric Research, the University of Colorado, and a grant from the IBM Shared University Research (SUR) program. Computing at Indiana University is supported by Lilly Endowment, Inc., through its support for the Indiana University Pervasive Technology Institute.

This work was supported in part by the U.S. Department of Energy under grants No. DE-FG02-91ER40628 (C.B., N.B.), No. DE-FC02-12ER41879 (C.D.), No. DE-SC0010120 (S.G.), No. DE-FG02-91ER40661 (S.G.), No. DE-FG02-13ER42001 (A.X.K.), No. DE-SC0015655 (A.X.K.), No. DE-SC0010005 (E.T.N.), No. DE-FG02-13ER41976 (D.T.); by the U.S. National Science Foundation under grants PHY14-14614 and PHY17-19626 (C.D.), PHY14-17805 (J.L.), and PHY13-16748 and PHY16-20625 (R.S.); by the MINECO (Spain) under grants FPA2013-47836-C-1-P and FPA2016-78220-C3-3-P (E.G.); by the Junta de Andalucía (Spain) under grant No. FQM-101 (E.G.); by the DFG cluster of excellence "Origin and Structure of the Universe" (N.B., A.V.); by the UK Science and Technology Facilities Council (J.K.); by the German Excellence Initiative and the European Union Seventh Framework Program under grant agreement No. 291763 as well as the European Union's Marie Curie COFUND program (J.K., A.S.K.). Brookhaven National Laboratory is supported by the United States Department of Energy, Office of Science, Office of High Energy Physics, under Contract No. DE-SC0012704. This document was prepared by the Fermilab Lattice, MILC, and TUMQCD Collaborations using the resources of the Fermi National Accelerator Laboratory (Fermilab), a U.S. Department of Energy, Office of Science, HEP User Facility. Fermilab is managed by Fermi Research Alliance, LLC (FRA), acting under Contract No. DE-AC02-07CH11359.

Appendix A: Correlation matrices

We report in Table III the correlation matrix of the MRS masses of the charm and bottom quarks with the HQET matrix elements, and in Table IV the correlation matrix for our charm-quark mass and quark-mass ratios. Knowledge of these correlations may be useful for future phenomenological studies.

[1] N. Brambilla, J. Komijani, A. S. Kronfeld, and A. Vairo (TUMQCD), Phys. Rev. **D97**, 034503 (2018), arXiv:1712.04983 [hep-ph].

TABLE III. Correlation matrix between the MRS masses of the charm and bottom quarks and HQET matrix elements; entries are symmetric across the diagonal. The last row gives the central value and total uncertainty (added in quadrature) of each quantity.

	$m_{c,\mathrm{MRS}}$	$m_{b,\mathrm{MRS}}$	$\overline{\Lambda}_{\mathrm{MRS}}$	μ_π^2	$\mu_G^2(m_b)$
$m_{c,\mathrm{MRS}}$	1				
$m_{b,\mathrm{MRS}}$	0.73277257	1			
$\overline{\Lambda}_{\mathrm{MRS}}$	0.13639123	−0.24098013	1		
μ_π^2	−0.09926990	0.56508134	−0.57458680	1	
$\mu_G^2(m_b)$	−0.37442069	0.01284048	−0.10454595	0.58306118	1
	1393(13) MeV	4751(18) MeV	552(30) MeV	0.06(22) GeV^2	0.38(2) GeV^2

TABLE IV. Correlation matrix between $m_{c,\overline{\mathrm{MS}}}(3\ \mathrm{GeV})$ and quark mass ratios; entries are symmetric across the diagonal. The last row gives the central value and total uncertainty (added in quadrature) of each quantity.

	$m_{c,\overline{\mathrm{MS}}}(3\ \mathrm{GeV})$	m_b/m_c	m_s/m_c	m_d/m_c	m_u/m_c
$m_{c,\overline{\mathrm{MS}}}(3\ \mathrm{GeV})$	1				
m_b/m_c	−0.58781239	1			
m_s/m_c	−0.05491365	0.36926569	1		
m_d/m_c	0.14642328	0.02901347	0.32767193	1	
m_u/m_c	−0.16904381	0.20362766	0.34027098	−0.51522822	1
	984.3(5.6) MeV	4.577(8)	0.08486(16)	0.004301(36)	0.001943(34)

[2] Q. Mason, H. D. Trottier, R. Horgan, C. T. H. Davies, and G. P. Lepage (HPQCD), Phys. Rev. **D73**, 114501 (2006), hep-ph/0511160.

[3] A. Skouroupathis and H. Panagopoulos, Phys. Rev. **D79**, 094508 (2009), arXiv:0811.4264 [hep-lat].

[4] M. Constantinou, M. Hadjiantonis, H. Panagopoulos, and G. Spanoudes, Phys. Rev. **D94**, 114513 (2016), arXiv:1610.06744 [hep-lat].

[5] G. Martinelli, C. Pittori, C. T. Sachrajda, M. Testa, and A. Vladikas, Nucl. Phys. **B445**, 81 (1995), hep-lat/9411010.

[6] A. T. Lytle and S. R. Sharpe, Phys. Rev. **D88**, 054506 (2013), arXiv:1306.3881 [hep-lat].

[7] S. Capitani, M. Lüscher, R. Sommer, and H. Wittig, Nucl. Phys. **B544**, 669 (1999), (E) Nucl. Phys. **B582**, 762 (2000), hep-lat/9810063.

[8] M. Della Morte, R. Hoffmann, F. Knechtli, J. Rolf, R. Sommer, I. Wetzorke, and U. Wolff (ALPHA), Nucl. Phys. **B729**, 117 (2005), hep-lat/0507035.

[9] I. Allison *et al.* (HPQCD), Phys. Rev. **D78**, 054513 (2008), arXiv:0805.2999 [hep-lat].

[10] W. A. Bardeen, A. J. Buras, D. W. Duke, and T. Muta, Phys. Rev. **D18**, 3998 (1978).

[11] E. D. Freeland, A. S. Kronfeld, J. N. Simone, and R. S. Van de Water (Fermilab Lattice), PoS **LAT2006**, 083 (2006), hep-lat/0610108; **LAT2007**, 243 (2007), arXiv:0710.4339 [hep-lat].

[12] P. Gambino, A. Melis, and S. Simula, Phys. Rev. **D96**, 014511 (2017), arXiv:1704.06105 [hep-lat].

[13] A. S. Kronfeld and J. N. Simone, Phys. Lett. **B490**, 228 (2000), (E) Phys. Lett. **B495**, 441 (2000), hep-ph/0006345.
[14] A. Bazavov *et al.*, (2017), arXiv:1712.09262 [hep-lat].
[15] A. F. Falk and M. Neubert, Phys. Rev. **D47**, 2965 (1993), hep-ph/9209268.
[16] A. G. Grozin, P. Marquard, J. H. Piclum, and M. Steinhauser, Nucl. Phys. **B789**, 277 (2008), arXiv:0707.1388 [hep-ph].
[17] A. S. Kronfeld, Phys. Rev. **D58**, 051501 (1998), hep-ph/9805215.
[18] J. C. Breckenridge, M. J. Lavelle, and T. G. Steele, Z. Phys. **C65**, 155 (1995), hep-th/9407028.
[19] I. I. Bigi, M. A. Shifman, N. G. Uraltsev, and A. I. Vainshtein, Phys. Rev. **D50**, 2234 (1994), hep-ph/9402360.
[20] M. Beneke and V. M. Braun, Nucl. Phys. **B426**, 301 (1994), hep-ph/9402364.
[21] M. Beneke, Phys. Lett. **B344**, 341 (1995), hep-ph/9408380.
[22] A. Pineda, JHEP **06**, 022 (2001), hep-ph/0105008.
[23] J. Komijani, JHEP **08**, 062 (2017), arXiv:1701.00347 [hep-ph].
[24] C. Bernard and J. Komijani, Phys. Rev. **D88**, 094017 (2013), arXiv:1309.4533 [hep-lat].
[25] A. Bazavov *et al.* (MILC), Phys. Rev. **D82**, 074501 (2010), arXiv:1004.0342 [hep-lat].
[26] A. Bazavov *et al.* (MILC), Phys. Rev. **D87**, 054505 (2013), arXiv:1212.4768 [hep-lat].
[27] A. Bazavov *et al.* (MILC), PoS **LATTICE2008**, 033 (2008), [arXiv:0903.0874]; PoS **LAT2009**, 123 (2009) [arXiv:0911.0869]; PoS **LATTICE2010**, 320 (2010) [arXiv:1012.1265].
[28] E. Follana, Q. Mason, C. Davies, K. Hornbostel, G. P. Lepage, J. Shigemitsu, H. Trottier, and K. Wong (HPQCD), Phys. Rev. **D75**, 054502 (2007), hep-lat/0610092.
[29] A. Hart, G. M. von Hippel, and R. R. Horgan (HPQCD), Phys. Rev. **D79**, 074008 (2009), arXiv:0812.0503 [hep-lat].
[30] M. G. Alford, W. Dimm, G. P. Lepage, G. Hockney, and P. B. Mackenzie, Phys. Lett. **B361**, 87 (1995), hep-lat/9507010.
[31] P. Weisz, Nucl. Phys. **B212**, 1 (1983).
[32] P. Weisz and R. Wohlert, Nucl. Phys. **B236**, 397 (1984), (E) Nucl. Phys. **B247**, 544 (1984).
[33] G. Curci, P. Menotti, and G. Paffuti, Phys. Lett. **130B**, 205 (1983), (E) Phys. Lett. **135B**, 516 (1984).
[34] M. Lüscher and P. Weisz, Commun. Math. Phys. **97**, 59 (1985), (E) Commun. Math. Phys. **98**, 433 (1985).
[35] M. Lüscher and P. Weisz, Phys. Lett. **158B**, 250 (1985).
[36] E. Marinari, G. Parisi, and C. Rebbi, Nucl. Phys. **B190**, 734 (1981).
[37] E. Follana, A. Hart, and C. T. H. Davies (HPQCD), Phys. Rev. Lett. **93**, 241601 (2004), hep-lat/0406010.
[38] S. Dürr, C. Hoelbling, and U. Wenger, Phys. Rev. **D70**, 094502 (2004), hep-lat/0406027.
[39] S. Dürr and C. Hoelbling, Phys. Rev. **D71**, 054501 (2005), hep-lat/0411022.
[40] K. Y. Wong and R. M. Woloshyn, Phys. Rev. **D71**, 094508 (2005), hep-lat/0412001.
[41] Y. Shamir, Phys. Rev. **D71**, 034509 (2005), hep-lat/0412014.
[42] S. Prelovsek, Phys. Rev. **D73**, 014506 (2006), hep-lat/0510080.
[43] C. Bernard, Phys. Rev. **D73**, 114503 (2006), hep-lat/0603011.
[44] S. Dürr and C. Hoelbling, Phys. Rev. **D74**, 014513 (2006), hep-lat/0604005.
[45] C. Bernard, M. Golterman, and Y. Shamir, Phys. Rev. **D73**, 114511 (2006), hep-lat/0604017.
[46] Y. Shamir, Phys. Rev. **D75**, 054503 (2007), hep-lat/0607007.

[47] C. Bernard, C. E. DeTar, Z. Fu, and S. Prelovsek, Phys. Rev. **D76**, 094504 (2007), arXiv:0707.2402 [hep-lat].
[48] A. S. Kronfeld, PoS **LAT2007**, 016 (2007), arXiv:0711.0699 [hep-lat].
[49] G. C. Donald, C. T. H. Davies, E. Follana, and A. S. Kronfeld (HPQCD, Fermilab Lattice), Phys. Rev. **D84**, 054504 (2011), arXiv:1106.2412 [hep-lat].
[50] A. Bazavov *et al.* (Fermilab Lattice, MILC), Phys. Rev. **D90**, 074509 (2014), arXiv:1407.3772 [hep-lat]; PoS **LATTICE2014**, 382 (2014), arXiv:1411.2667 [hep-lat].
[51] J. Komijani *et al.* (Fermilab Lattice, MILC, TUMQCD), PoS **LATTICE2016**, 294 (2016), arXiv:1611.07411 [hep-lat].
[52] C. Patrignani *et al.* (Particle Data Group), Chin. Phys. **C40**, 100001 (2016); J. L. Rosner, S. Stone, and R. S. Van de Water, (2015), arXiv:1509.02220 [hep-ph].
[53] K. Symanzik, "Cutoff Dependence in Lattice ϕ_4^4 Theory," in *Recent developments in gauge theories*, edited by G. t Hooft *et al.* (Plenum, New York, 1980) p. 313.
[54] K. Symanzik, Nucl. Phys. **B226**, 187 (1983).
[55] C. G. Boyd and B. Grinstein, Nucl. Phys. **B442**, 205 (1995), hep-ph/9402340.
[56] A. V. Manohar and M. B. Wise, *Heavy Quark Physics* (Cambridge, Cambridge, UK, 2000).
[57] P. A. Baikov, K. G. Chetyrkin, and J. H. Kühn, JHEP **10**, 076 (2014), arXiv:1402.6611 [hep-ph].
[58] P. A. Baikov, K. G. Chetyrkin, and J. H. Kühn, Phys. Rev. Lett. **118**, 082002 (2017), arXiv:1606.08659 [hep-ph].
[59] P. Marquard, A. V. Smirnov, V. A. Smirnov, and M. Steinhauser, Phys. Rev. Lett. **114**, 142002 (2015), arXiv:1502.01030 [hep-ph].
[60] P. Marquard, A. V. Smirnov, V. A. Smirnov, M. Steinhauser, and D. Wellmann, Phys. Rev. **D94**, 074025 (2016), arXiv:1606.06754 [hep-ph].
[61] P. Ball, M. Beneke, and V. M. Braun, Nucl. Phys. **B452**, 563 (1995), hep-ph/9502300.
[62] C. Ayala, G. Cvetič, and A. Pineda, JHEP **09**, 045 (2014), arXiv:1407.2128 [hep-ph].
[63] S. Basak *et al.* (MILC), (2018), in preparation, and private communication by C. Bernard.
[64] S. Borsanyi *et al.* (Budapest-Marseille-Wuppertal), Phys. Rev. Lett. **111**, 252001 (2013), arXiv:1306.2287 [hep-lat].
[65] J. L. Rosner and M. B. Wise, Phys. Rev. **D47**, 343 (1993).
[66] J. L. Goity and C. P. Jayalath, Phys. Lett. **B650**, 22 (2007), hep-ph/0701245.
[67] C. T. H. Davies, C. McNeile, E. Follana, G. P. Lepage, H. Na, and J. Shigemitsu (HPQCD), Phys. Rev. **D82**, 114504 (2010), arXiv:1008.4018 [hep-lat].
[68] G. P. Lepage, B. Clark, C. T. H. Davies, K. Hornbostel, P. B. Mackenzie, C. Morningstar, and H. Trottier, Nucl. Phys. Proc. Suppl. **106**, 12 (2002), hep-lat/0110175.
[69] P. Gambino and C. Schwanda, Phys. Rev. **D89**, 014022 (2014), arXiv:1307.4551 [hep-ph].
[70] A. Bazavov *et al.* (Fermilab Lattice, MILC), Phys. Rev. **D85**, 114506 (2012), arXiv:1112.3051 [hep-lat].
[71] B. Chakraborty, C. T. H. Davies, B. Galloway, P. Knecht, J. Koponen, G. C. Donald, R. J. Dowdall, G. P. Lepage, and C. McNeile (HPQCD), Phys. Rev. **D91**, 054508 (2015), arXiv:1408.4169 [hep-lat]; private communication (2017).
[72] R. D. Ball, L. Del Debbio, S. Forte, A. Guffanti, J. I. Latorre, J. Rojo, and M. Ubiali (NNPDF), JHEP **05**, 075 (2010), arXiv:0912.2276 [hep-ph].
[73] C. Bernard and D. Toussaint (MILC), (2017), arXiv:1707.05430 [hep-lat].
[74] S. Aoki *et al.*, Eur. Phys. J. **C77**, 112 (2017), arXiv:1607.00299 [hep-lat].
[75] T. Liu and M. Steinhauser, Phys. Lett. **B746**, 330 (2015), arXiv:1502.04719 [hep-ph].

[76] M. Neubert, Phys. Lett. **B393**, 110 (1997), hep-ph/9610471.
[77] N. Uraltsev, Nucl. Phys. **B491**, 303 (1997), hep-ph/9610425.
[78] N. Uraltsev, Phys. Lett. **B545**, 337 (2002), hep-ph/0111166.
[79] N. Uraltsev, Phys. Lett. **B585**, 253 (2004), hep-ph/0312001.
[80] A. Alberti, P. Gambino, K. J. Healey, and S. Nandi, Phys. Rev. Lett. **114**, 061802 (2015), arXiv:1411.6560 [hep-ph].
[81] G. S. Bali and A. Pineda, Phys. Rev. **D69**, 094001 (2004), hep-ph/0310130.
[82] C. Alexandrou, V. Drach, K. Jansen, C. Kallidonis, and G. Koutsou, Phys. Rev. **D90**, 074501 (2014), arXiv:1406.4310 [hep-lat].
[83] N. Carrasco *et al.* (European Twisted Mass), Nucl. Phys. **B887**, 19 (2014), arXiv:1403.4504 [hep-lat].
[84] Y. Maezawa and P. Petreczky, Phys. Rev. **D94**, 034507 (2016), arXiv:1606.08798 [hep-lat].
[85] K. Nakayama, B. Fahy, and S. Hashimoto (JLQCD), Phys. Rev. **D94**, 054507 (2016), arXiv:1606.01002 [hep-lat].
[86] Y.-B. Yang *et al.* (χQCD), Phys. Rev. **D92**, 034517 (2015), arXiv:1410.3343 [hep-lat].
[87] C. McNeile, C. T. H. Davies, E. Follana, K. Hornbostel, and G. P. Lepage (HPQCD), Phys. Rev. **D82**, 034512 (2010), arXiv:1004.4285 [hep-lat].
[88] V. Mateu and P. G. Ortega, JHEP **01**, 122 (2018), arXiv:1711.05755 [hep-ph].
[89] K. G. Chetyrkin, J. H. Kühn, A. Maier, P. Maierhofer, P. Marquard, M. Steinhauser, and C. Sturm, Phys. Rev. **D96**, 116007 (2017), arXiv:1710.04249 [hep-ph].
[90] Y. Kiyo, G. Mishima, and Y. Sumino, Phys. Lett. **B752**, 122 (2016), (E) Phys. Lett. **B772**, 878 (2017), arXiv:1510.07072 [hep-ph].
[91] B. Dehnadi, A. H. Hoang, and V. Mateu, JHEP **08**, 155 (2015), arXiv:1504.07638 [hep-ph].
[92] S. Narison, Phys. Lett. **B706**, 412 (2012), arXiv:1105.2922 [hep-ph].
[93] S. Bodenstein, J. Bordes, C. A. Dominguez, J. Penarrocha, and K. Schilcher, Phys. Rev. **D83**, 074014 (2011), arXiv:1102.3835 [hep-ph].
[94] R. Boughezal, M. Czakon, and T. Schutzmeier, Phys. Rev. **D74**, 074006 (2006), hep-ph/0605023.
[95] A. Bussone *et al.* (ETM), Phys. Rev. **D93**, 114505 (2016), arXiv:1603.04306 [hep-lat].
[96] B. Colquhoun, R. J. Dowdall, C. T. H. Davies, K. Hornbostel, and G. P. Lepage (HPQCD), Phys. Rev. **D91**, 074514 (2015), arXiv:1408.5768 [hep-lat].
[97] A. J. Lee, C. J. Monahan, R. R. Horgan, C. T. H. Davies, R. J. Dowdall, and J. Koponen (HPQCD), Phys. Rev. **D87**, 074018 (2013), arXiv:1302.3739 [hep-lat].
[98] C. Ayala, G. Cvetič, and A. Pineda, J. Phys. Conf. Ser. **762**, 012063 (2016), arXiv:1606.01741 [hep-ph].
[99] M. Beneke, A. Maier, J. Piclum, and T. Rauh, PoS **RADCOR2015**, 035 (2016), arXiv:1601.02949 [hep-ph]; Nucl. Phys. **B891**, 42 (2015), arXiv:1411.3132 [hep-ph].
[100] A. A. Penin and N. Zerf, JHEP **04**, 120 (2014), arXiv:1401.7035 [hep-ph].
[101] S. Bodenstein, J. Bordes, C. A. Dominguez, J. Penarrocha, and K. Schilcher, Phys. Rev. **D85**, 034003 (2012), arXiv:1111.5742 [hep-ph].
[102] K. G. Chetyrkin, J. H. Kühn, A. Maier, P. Maierhofer, P. Marquard, M. Steinhauser, and C. Sturm, Phys. Rev. **D80**, 074010 (2009), arXiv:0907.2110 [hep-ph].
[103] N. Brambilla, Y. Sumino, and A. Vairo, Phys. Rev. **D65**, 034001 (2002), hep-ph/0108084.
[104] T. Blum *et al.* (RBC, UKQCD), Phys. Rev. **D93**, 074505 (2016), arXiv:1411.7017 [hep-lat].
[105] S. Dürr, Z. Fodor, C. Hoelbling, S. D. Katz, S. Krieg, T. Kurth, L. Lellouch, T. Lippert, K. K. Szabo, and G. Vulvert (Budapest-Marseille-Wuppertal), Phys. Lett. **B701**, 265 (2011),

arXiv:1011.2403 [hep-lat].
[106] A. Bazavov *et al.* (MILC), PoS **CD09**, 007 (2009), arXiv:0910.2966 [hep-ph]; A. Bazavov *et al.*, Rev. Mod. Phys. **82**, 1349 (2010), arXiv:0903.3598 [hep-lat].
[107] J. Towns, T. Cockerill, M. Dahan, I. Foster, K. Gaither, A. Grimshaw, V. Hazlewood, S. Lathrop, D. Lifka, G. D. Peterson, R. Roskies, J. R. Scott, and N. Wilkins-Diehr, Computing in Science & Engineering **16**, 62 (2014).